Cell Reports

Article

ZBP1 pathway promotes tumor immunogenicity in the combination of anti-HER2 therapy and epigenetic therapy

Graphical abstract

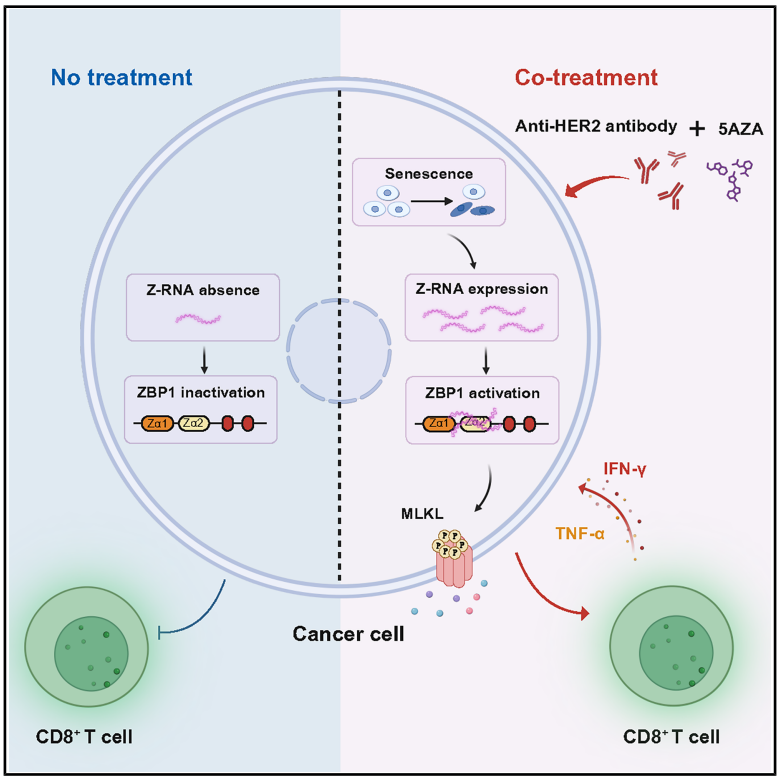

Highlights

- Epigenetic therapy sensitizes HER2 targeted intervention and promotes tumor control
- Tumor intrinsic ZBP1 facilitates CD8$^+$ T cell responses of combination therapy
- STAT1 mediates ZBP1 activation following 5AZA or synergized treatment
- Increased Z-RNA gathering in senescent tumor cells boosts ZBP1 activation

Authors

Qishan Wang, Zhihao Wu, Yuanqin Yang, ..., Xueni Yu, Lu Lu, Liufu Deng

Correspondence

lulu0113@sjtu.edu.cn (L.L.), dengliufu@sjtu.edu.cn (L.D.)

In brief

Wang et al. demonstrate that 5AZA combined with anti-HER2 therapy enhances tumor immunogenicity via ZBP1 activation. Increased accumulation of Z-RNA during senescence promotes ZBP1 activation. Epigenetic modulation represents a promising therapeutic strategy to sensitize anti-HER2 immunotherapy.

Wang et al., 2025, Cell Reports *44*, 116314
October 28, 2025
https://doi.org/10.1016/j.celrep.2025.116314

CellPress

Cell Reports

CellPress
OPEN ACCESS

Article

ZBP1 pathway promotes tumor immunogenicity in the combination of anti-HER2 therapy and epigenetic therapy

Qishan Wang,[1,2] Zhihao Wu,[1,2] Yuanqin Yang,[1] Chao Yang,[1] Haoran Deng,[1] Xingyue Zhou,[1] Shuting Xu,[1] Lingling Wu,[1] Xiaochuan Hong,[1] Xueni Yu,[1] Lu Lu,[1,*] and Liufu Deng[1,3,*]

[1]Shanghai Frontiers Science Center of Drug Target Identification and Delivery, State Key Laboratory of Innovative Immunotherapy, School of Pharmaceutical Sciences, Shanghai Jiao Tong University, Shanghai 200240, China

[2]These authors contributed equally

[3]Lead contact

*Correspondence: lulu0113@sjtu.edu.cn (L.L.), dengliufu@sjtu.edu.cn (L.D.)

https://doi.org/10.1016/j.celrep.2025.116314

SUMMARY

Z-form DNA (Z-DNA)-binding protein 1 (ZBP1)-mediated RNA sensing plays a critical role in tumor immunogenicity. However, how to augment ZBP1 signaling-mediated immunogenic tumor cell death to boost targeted therapy is yet unknown. Here, we demonstrated that epigenetic modulation by 5-aza-2′-deoxycytidine (5AZA) facilitated antitumor effects of anti-HER2 therapy, which requires antitumor $CD8^+$ T cell responses initiated by ZBP1-mediated tumor immunogenicity. Moreover, the combination of anti-HER2 and 5AZA induced increased ZBP1 expression and related Z-RNA enrichment in tumor cells, leading to the activation of ZBP1 via Z-RNA bound to the Zα2 domain. Particularly, the accumulation of Z-RNA is largely sequestered in senescent tumor cells, which presumably allows prolonged Z-RNA sensing. Therefore, our study indicates that ZBP1-mediated Z-RNA sensing acts as a key determinant of targeted therapy combined with epigenetic therapy through bridging tumor stress responses with antitumor adaptive immunity, providing insights into the development of innate immune sensing-based immunotherapeutic strategies for cancer treatment.

INTRODUCTION

Human epidermal growth factor receptor 2 (HER2) is overexpressed in 20%–30% of breast cancer (BRCA) and various other carcinomas. Inhibiting HER2 forces malignant cells to rely on alternative or mutated survival pathways.[1] However, accumulating researches have highlighted the significant role of the host and the tumor microenvironment (TME) in driving therapeutic resistance. The development of resistance is influenced by both the intrinsic properties of cancer cells and the extrinsic factors from the host immunity.[2] In HER2-amplified BRCA, the phosphatidylinositol 3-kinase (PI3K)-protein kinase B (AKT)-mammalian target of rapamycin (mTOR) pathway promotes an inflammatory phenotype that leads to interleukin-8 secretion, enhancing malignancy and therapeutic resistance.[3,4] Besides, HER2 also dampens antitumor innate immune responses by inhibiting TANK-binding kinase 1 (TBK1) phosphorylation and the stimulator of interferon genes (STING) signaling pathway.[5] Although anti-HER2 antibody treatments often elicit tumor regression through oncogenic signal inhibition and Fc receptor (FcR)-mediated cytotoxicity, the engagement of $CD8^+$ T cells from the adaptive immune system is indispensable.[1] However, how to improve anti-HER2 therapy from the angle of innate immune sensing remains unknown.

$CD8^+$ T cells play a pivotal role in antitumor immunity.[6] Tumors can be classified into "hot" and "cold" tumors according to T cell infiltration. "Hot tumors" exhibit inherent immunogenicity, characterized by the damage-associated molecular pattern (DAMP)-mediated DNA and RNA sensing pathway activation, which enhances antitumor immunity.[7] Studies have shown that cyclic GMP-AMP synthase (cGAS) expression in cancer cells and CBL0137-induced Z-form DNA (Z-DNA) accumulation in the TME promote $CD8^+$ T cell recruitment.[7,8] Z-RNA-mediated tumor immunogenicity, which is suppressed by ADAR1, is also a promising strategy to exploit $CD8^+$ T cell immunity.[8] Leveraging nucleic acid sensing-induced immunogenicity enhances $CD8^+$ T cell antitumor responses. Immunogenic cell death (ICD) and senescence are both effective strategies to strengthen tumor immunogenicity. Necroptosis, a form of ICD, releases DAMPs that trigger sustained immune responses via tumor necrosis factor (TNF), pattern recognition receptors (PRRs), Toll-like receptor 4 (TLR4), and Z-DNA-binding protein 1 (ZBP1).[9] Our previous study has shown that the ZBP1-mixed-lineage kinase-like (MLKL) pathway is necessary for maintaining $CD8^+$ T cell functions in radiation-treated tumors. Tumor clearance is mediated by interferon (IFN)-γ-producing $CD8^+$ T cells specific to tumor antigens.[10–12] Senescence has been found to be even more immunogenic than ICD, further reinforcing $CD8^+$ T cell-driven antitumor immunity.[13] Epigenetic therapy, such as EZH2 inhibitors, sensitizes senescence-activating therapy by augmenting senescence and promoting NK

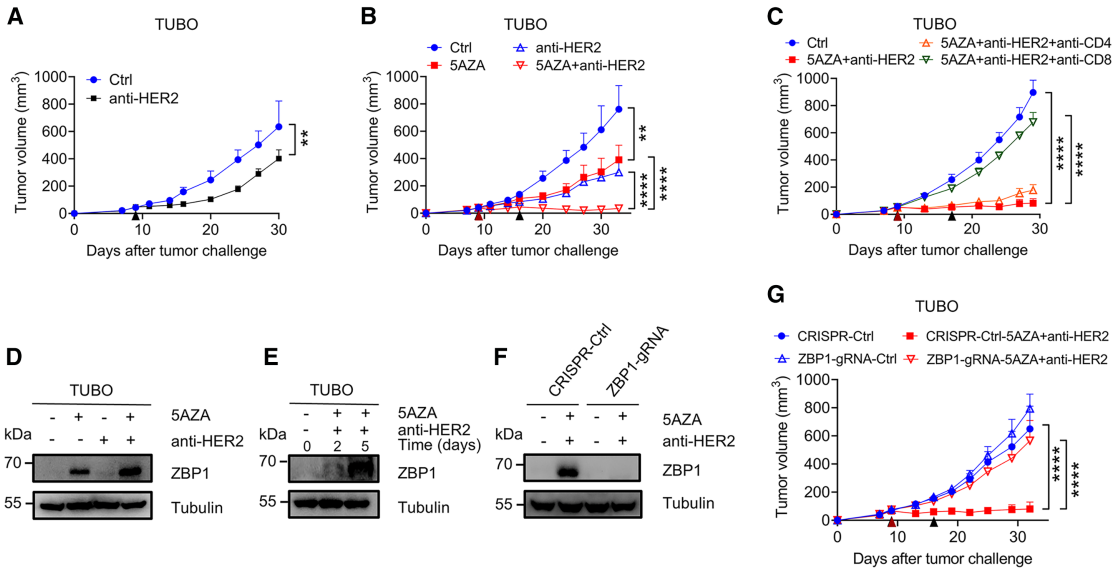

Figure 1. Anti-HER2 mAb and 5AZA synergistically promotes tumor control in a ZBP1-dependent manner

(A) Tumor growth of TUBO cells following treatment with anti-HER2 antibodies. The black arrows indicate anti-HER2 mAb therapy (n = 5).

(B) Combination therapy with anti-HER2 mAb and 5AZA suppressed TUBO tumor growth. The black arrows indicate 5AZA or anti-HER2 mAb monotherapy, and the red arrow indicates combination therapy of anti-HER2 mAb and 5AZA (n = 5).

(C) $CD8^+$ T cells mediated essential efficacy of combination therapy in TUBO tumors (n = 5).

(D and E) ZBP1 activation after combination therapy of anti-HER2 mAb and 5AZA in TUBO cells.

(F and G) 5AZA in combination with anti-HER2 mAb-mediated therapeutic effects depended on ZBP1 presence in TUBO tumors. TUBO cells were collected on day 5 for western blot (G: n = 5). Data are represented as means ± SEM. $^{**}p < 0.01$ and $^{****}p < 0.0001$ by two-way ANOVA in (A–C and G). See also Figure S1.

and T cell functions.[14] However, the relationship between cellular senescence and Z-RNA sensing in tumor immunogenicity is still largely unexplored. Thus, the approach to optimize anti-HER2 therapy for promoting intrinsic tumor immunogenicity to enhance the $CD8^+$ T cell response is not fully understood.

Cytosolic nucleic acids, particularly double-stranded RNA (dsRNA) from endogenous retroviruses (ERVs), activate potent innate immunity through mechanisms such as SET domain bifurcated histone lysine methyltransferase 1 (SETDB1) ablation and epigenetic therapy.[15–17] DsRNA can form either a right-handed or left-handed double helix (Z-RNA), the latter of which is less well understood due to its bioenergetically unfavorable conformation.[18] Z-RNA is recognized by the ZBP1 Zα domain, which mediates innate immune responses and necroptotic cell death.[19–21] The accumulation of Z-RNA, which activates ZBP1, is regulated by both ADAR1 depletion and retroelement reactivation.[8,22] ZBP1 triggers host defense by Zα domain sensing, though Z-nucleic acid sensing is not required for ZBP1 activation under heat stress.[23] The role of ZBP1 in triggering tumor necroptosis and in reactive oxygen species (ROS)-induced Z-RNA generation for tumor control has been established.[22,24] However, there is no evidence of ZBP1 direct activation by Z-RNA under steady state due to low Z-RNA levels. Therefore, promoting tumor-derived Z-RNA formation may enhance immunogenicity. The epigenetic reprogramming agent 5-aza-2′-deoxycytidine (5AZA) has been demonstrated to induce dsRNA formation for debulking therapies.[25] Our previous study has shown that 5AZA monotherapy activates ZBP1.[12] However, it is essential to determine whether the combination of 5AZA treatment and anti-HER2 therapy impacts ZBP1-driven tumor immunogenicity.

In this work, we demonstrated that anti-HER2 combined with 5AZA significantly suppressed tumor growth by activating ZBP1, which binds Z-RNA through the Zα2 domain. Correspondingly, the increased accumulation of Z-RNA during senescence allows ZBP1 activation. Therefore, we propose that epigenetic modulation enhances antitumor $CD8^+$ T cell responses to anti-HER2 therapy through ZBP1-driven tumor immunogenicity.

RESULTS

Anti-HER2 therapy and 5AZA synergistically promote tumor control through converging on a ZBP1-dependent manner

Therapeutic resistance emerged in the tumor growth of TUBO cells following treatment with anti-HER2 antibodies (Figure 1A). 5AZA is a specified DNA methyltransferase (DNMT) inhibitor. Given that its clinical doses are often cytotoxic and not optimized for epigenetic therapy, we used low doses of 5AZA as a synergetic epigenetic modulator with anti-HER2 antibodies.[17,25] TUBO is a HER2/neu-dependent BRCA cell cloned from a spontaneous mammary tumor in a BALB/c Neu-transgenic mouse.[26] The combination therapy of anti-HER2 monoclonal antibody (mAb) and 5AZA displayed better tumor control compared to either anti-HER2 mAb or epigenetic intervention alone (Figures 1B and S1A). To further delineate whether adaptive immunity was required for tumor regression induced by combination therapy, we depleted $CD8^+$ T cells or $CD4^+$ T cells in

TUBO-bearing mice alongside the combination therapy (Figure S1B). We found that $CD8^+$ T cells ablation abolished the antitumor activity of the combination therapy, while $CD4^+$ T cells depletion had no impact on tumor regression (Figure 1C). Taken together, these data demonstrate that 5AZA synergizes with anti-HER2 mAb to suppress tumor growth and that this efficacy is driven by $CD8^+$ T cells rather than $CD4^+$ T cells.

In our previous study, pan-cancer analysis of 31 malignancies from The Cancer Genome Atlas (TCGA) demonstrated a significant positive correlation between ZBP1 expression and $CD8^+$ T cell infiltration levels, with the most pronounced association observed in HER2-enriched BRCA.[12] The Gene Expression Profiling Interaction Analysis (GEPIA) also showed that $HER2^+$ BRCA patients with high ZBP1 expression exhibited improved overall survival, suggesting the possibility that ZBP1 expression may be correlated with $HER2^+$ BRCA response to therapies (Figure S1C).

To further validate the critical role of ZBP1 in the therapeutic efficacy of anti-HER2 mAb combined with 5AZA, we first measured the ZBP1 protein level following different treatments. We found that 5AZA treatment alone increased ZBP1 expression, while anti-HER2 antibody alone did not induce ZBP1 expression. Notably, the combination treatment resulted in a more robust ZBP1 accumulation compared to 5AZA alone (Figure 1D). Additionally, the combination treatment promoted ZBP1 expression in a time-dependent manner (Figure 1E). To determine whether the tumor intrinsic ZBP1 is essential for the antitumor effect of combination treatment, we generated ZBP1 deficiency TUBO cell line. ZBP1 deficiency did not influence the cell growth rate of tumor cells *in vitro* (Figures 1F and S1D). Tumor growth analysis showed that ZBP1 deficiency tumors displayed notably greater resistance to the antitumor effects of combination therapy (Figure 1G). Moreover, ZBP1 deficiency also diminished the antitumor effects of 5AZA monotherapy (Figure S1E). Collectively, these results indicate that ZBP1 is required for the antitumor effects of 5AZA monotherapy and combination therapy.

Tumor cell-intrinsic ZBP1 facilitates antitumor T cell responses of the combination of anti-HER2 therapy and 5AZA treatment

Since anti-HER2 treatment did not induce ZBP1 expression, our subsequent investigations focus on both 5AZA monotherapy and combination treatment. Considering that TUBO tumor cells possess lower tumor immunogenicity, the MC38 tumor model with stronger immunogenicity was used to investigate whether tumor-intrinsic ZBP1 regulates antitumor immune response after 5AZA monotherapy. ZBP1 deficiency in MC38 cell line did not influence the tumor cell growth rate *in vitro* (Figure S2A). Compared with the CRISPR-Ctrl group, 5AZA therapy displayed robust antitumor effects, while ZBP1 knockout in tumors largely abrogated the difference, indicating that tumor cell-intrinsic ZBP1 is required for antitumor effects of 5AZA treatment (Figure 2A).

To evaluate the contribution of ZBP1 in tumor to $CD8^+$ T cell responses post 5AZA treatment, we used flow cytometry to quantify $CD8^+$ T cell effector functions and proliferation potential within the TME. Compared to the CRISPR-Ctrl group, the 5AZA-treated group showed higher expression levels of IFN-γ and Ki-67 antigen (Ki-67). However, $ZBP1^{-/-}$ tumors failed to increase $CD8^+$ T cell effector functions and proliferation potential after 5AZA therapy (Figures 2B, 2C, and S2B). To determine whether antigen-specific $CD8^+$ T cell dysfunction accounted for the lack of response to 5AZA treatment in ZBP1-deficient tumors, we performed an enzyme-linked immunospot (ELISPOT) assay for IFN-γ detection. ELISPOT assay showed that 5AZA treatment generated a potent tumor antigen-specific $CD8^+$ T cell response in CRISPR-Ctrl tumors, whereas an attenuated response was observed in $ZBP1^{-/-}$ tumors (Figures 2D and 2E). Furthermore, to evaluate the role of ZBP1 in mediating the response of exogenous $CD8^+$ T cells to 5AZA therapy, we conducted adoptive transfer of activated OT-I $CD8^+$ T cells into mice bearing either ZBP1-deficient or ZBP1-sufficient (CRISPR-Ctrl) MC38-OVA tumors (Figure 2F). Consistently, 5AZA treatment maintained a potent tumor-specific exogenous $CD8^+$ T cell response in CRISPR-Ctrl MC38-OVA tumors, whereas an impaired response was observed in ZBP1-deficient tumors (Figures 2G, 2H, and S2C). In conclusion, these data suggest that the tumor cell-intrinsic ZBP1 is required for the antitumor responses of $CD8^+$ T cells after 5AZA treatment.

In a less immunogenic TUBO cell line, 5AZA alone is inadequate for durable tumor regression, and the combination of 5AZA and anti-HER2 mAb was introduced. In the combination therapy group, the percentages of IFN-γ and TNF-α double-positive and Ki-67-positive $CD8^+$ T cells were higher than those in the groups treated with either anti-HER2 mAb or 5AZA alone (Figures 2I and 2J). Collectively, these findings suggest that the robust tumor regression observed with the combination therapy is primarily driven by the enhanced functionality of $CD8^+$ T cells. To further elucidate the immune cell landscape within tumors under synergistic treatment, we subsequently conducted flow cytometry analysis to distinguish various immune cell populations (Figure S2D). Compared with 5AZA monotherapy, the percentage of tumor-infiltrating $CD8^+$ T cells remained at comparable levels after combination therapy, suggesting that the enhanced $CD8^+$ T cell-mediated immune effects with combination treatment are primarily due to the augmented effector functions, rather than increased infiltration (Figure S2E). Indeed, the combination therapy resulted in an increase of dendritic cell (DC) infiltration in tumors, with upregulated expression of costimulatory molecules CD80 on intratumoral DCs (Figures S2F and S2G). This finding is indicative of enhanced DC functions and $CD8^+$ T cell responses. In addition, the infiltration of natural killer (NK) cells and $CD4^+$ T cells remained relatively unchanged under combination treatments (Figures S2H and S2I). Overall, our findings demonstrate that synergistic therapy combining anti-HER2 mAb and 5AZA primarily enhances the antitumor response through the augmented functionality of $CD8^+$ T cells. We next sought to assess whether tumor cell-intrinsic ZBP1 is indispensable for the $CD8^+$ T cell anti-tumor response of combination therapy. The results showed that the production of IFN-γ, TNF-α, and Ki-67 was compromised in ZBP1-deficient tumors compared to that in control ones (Figures 2K and 2L). Above all, tumor cell-intrinsic ZBP1 facilitates antitumor $CD8^+$ T cell responses in the combination treatment of 5AZA and anti-HER2 mAb.

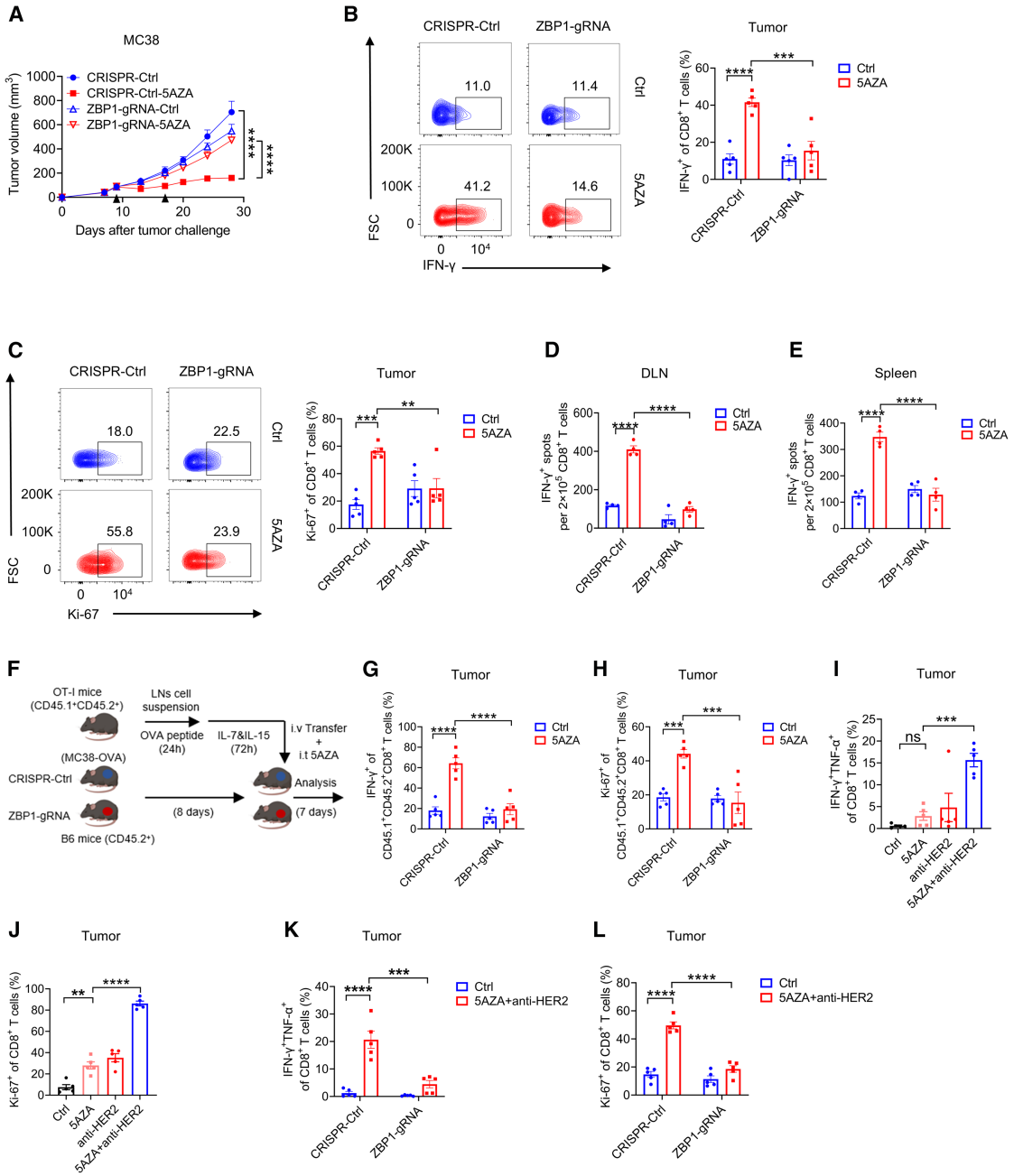

Figure 2. Tumor cell-intrinsic ZBP1 facilitates antitumor CD8$^+$ T cell responses in combination therapy of 5AZA and anti-HER2 mAb

(A) 5AZA-mediated therapeutic effects depended on ZBP1 presence in MC38 tumors. The black arrows indicate 5AZA monotherapy (n = 5).

(B and C) Function and proliferation markers of CD8$^+$ T cells from CRISPR-Ctrl and ZBP1$^{-/-}$ MC38 tumors on day 16 after 5AZA monotherapy (n = 5).

(D and E) Function of tumor antigen–specific CD8$^+$ T cells from the draining lymph nodes (DLNs) and spleen of MC38 tumors on day 16 after 5AZA monotherapy (n = 4).

(F) Schematic illustration of MC38-OVA tumor-bearing mice after 5AZA therapy and OT-I CD8$^+$ T cell therapy.

(G and H) Functions and proliferation potential of transferred CD8$^+$ T cells from MC38-OVA tumors on day 15 after 5AZA monotherapy (n = 5).

(I and J) Functions and proliferation potential of CD8$^+$ T cells in TUBO tumors on day 16 after indicated therapies (n = 5).

(K and L) Functions and proliferation potential of CD8$^+$ T cells from CRISPR-Ctrl and ZBP1$^{-/-}$ TUBO tumors on day 16 after indicated therapies (n = 5). Data are represented as means ± SEM. $^{**}p < 0.01$, $^{***}p < 0.001$, and $^{****}p < 0.0001$ by two-way ANOVA in (A) and one-way ANOVA in (B–E and G–L). See also Figure S2.

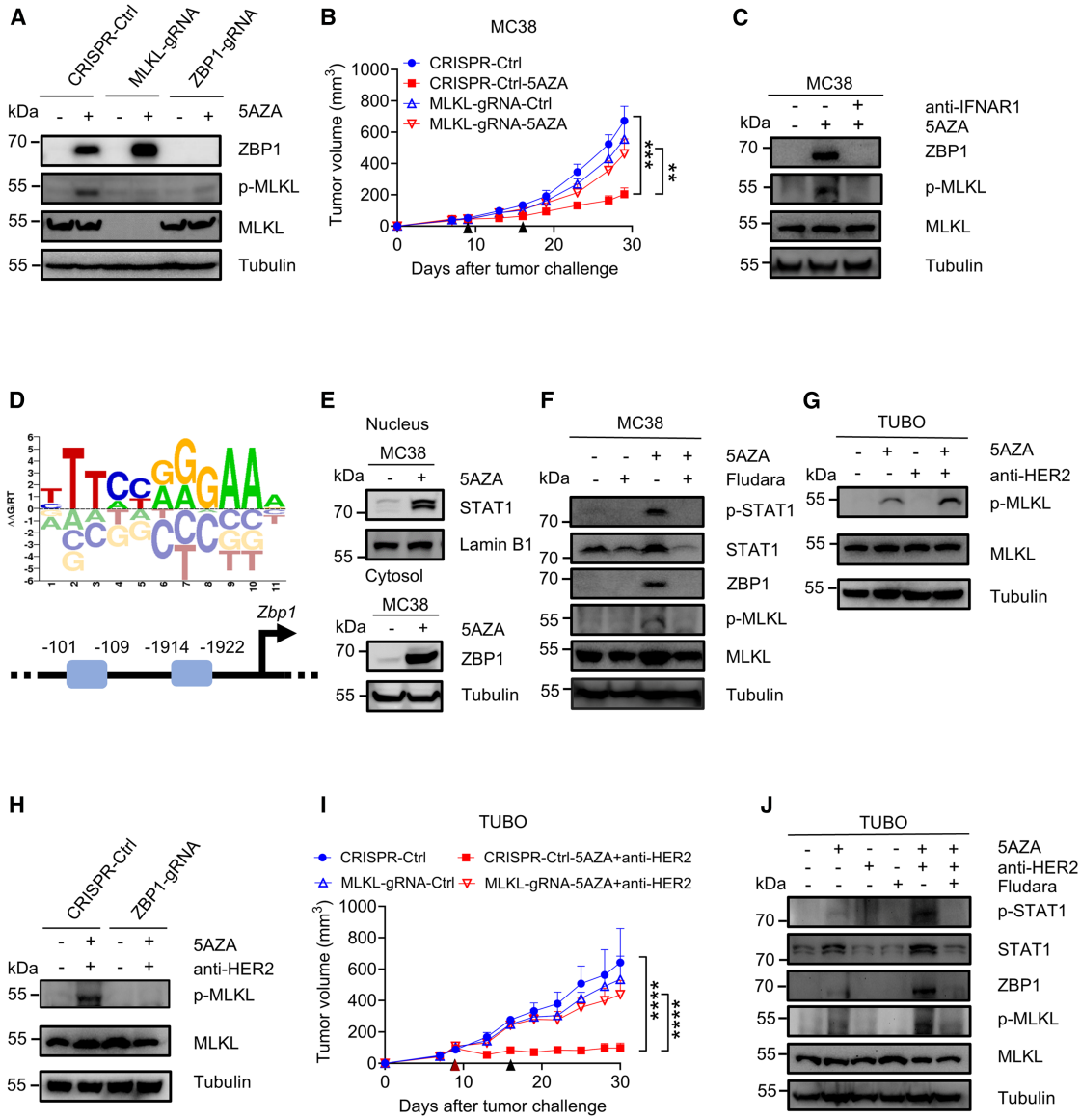

Figure 3. STAT1 mediates ZBP1 activation in response to 5AZA and combination therapy of 5AZA and anti-HER2 mAb

(A) Activation of the ZBP1-MLKL pathway after 5AZA treatment in MC38 cells on day 5.

(B) 5AZA-mediated therapeutic effects depended on MLKL presence in MC38 tumors. The black arrows indicate 5AZA monotherapy ($n = 5$).

(C) Blockage of type I interferon pathway inhibited ZBP1-MLKL cascade under 5AZA treatment in MC38 cells on day 5.

(D) The specific binding site of STAT1 in the ZBP1 promoter region predicted by the Jasper database and the AnimalTFBD database.

(E) Nuclear translocation of STAT1 under 5AZA treatment in MC38 cells on day 5.

(F) STAT1 inhibitor abolished ZBP1 activation after 5AZA treatment in MC38 cells on day 5.

(G) The activation of MLKL under combination therapy in TUBO cells on day 5.

(H) ZBP1 deficiency abrogated MLKL activation in TUBO cells on day 5.

(I) Therapeutic effects of synergized treatments depended on MLKL presence in TUBO tumors. The black arrows indicate 5AZA or anti-HER2 mAb monotherapy, and the red arrow indicates combination therapy ($n = 5$).

(J) STAT1 regulated the expression of ZBP1 protein after synergized treatments in TUBO cells on day 5. Data are represented as means ± SEM. $^{**}p < 0.01$, $^{***}p < 0.001$, and $^{****}p < 0.0001$ by two-way ANOVA in (B and I). See also Figure S3.

STAT1 mediates ZBP1 expression in response to 5AZA and combination treatments

ZBP1 triggers RIPK3-MLKL-dependent necroptosis and facilitates type I interferon responses to promote radiation-induced antitumor immunity.[12] We found that loss of ZBP1 or MLKL impaired MLKL phosphorylation and alleviated cell death induced by 5AZA treatment (Figures 3A and S3A). Similarly, MLKL knockout in MC38 tumors also resulted in negation of

the effects of 5AZA treatment, consistent with our observations in ZBP1-deficient MC38 tumors. These data indicate that tumor cell-intrinsic ZBP1-MLKL-mediated ICD is required for the antitumor effects of 5AZA treatment (Figure 3B). Besides, given that RIPK3 is frequently silenced in many tumor cells, rendering them resistant to necroptosis,[27] we determined whether MC38 and TUBO cell lines express RIPK3. Our results confirmed that RIPK3 expression was detectable in both cell lines (Figure S3B). ZBP1 is an interferon-inducible factor, and 5AZA up-regulated the expression of ZBP1 in a manner similar to that of type I interferon.[28] Blocking type I IFN production with anti-interferon alpha and beta receptor subunit 1 (anti-IFNAR1) antibody disrupted the ZBP1-MLKL pathway during 5AZA monotherapy (Figure 3C). Therefore, we hypothesize that the upregulation of ZBP1 in tumor cells treated with either 5AZA or combination therapy is associated with downstream transcriptional factor of the type I IFN pathway. The predicated data suggested that STAT1 regulated ZBP1 expression, with putative STAT1-binding sites identified in the ZBP1 promoter region (Figure 3D). Moreover, we observed the nuclear translocation of STAT1 in 5AZA-treated cells along with ZBP1 upregulation (Figure 3E). To further investigate the role of STAT1 in ZBP1-MLKL activation following 5AZA treatment, we used an inhibitor of STAT1, fludarabine, to dampen STAT1 function.[29] The STAT1 inhibitor abolished ZBP1-MLKL activation induced by 5AZA treatment (Figure 3F). Together, these findings provide evidence that STAT1 translocates to the nucleus to upregulate ZBP1 expression under 5AZA monotherapy.

To further explore the ZBP1-MLKL mediated tumor-intrinsic necroptosis pathway in combination therapy, TUBO cell lines were utilized. Compared to the 5AZA monotreatment group, the ZBP1-MLKL cascade was activated after combined induction, whereas the absence of ZBP1 inhibited MLKL phosphorylation and cell death (Figures 1D, 3G, 3H, and S3C). Tumor growth analysis showed that MLKL deficiency largely abrogated the antitumor effects of combination therapy (Figures 3I and S3D). These data suggest that tumor cell-intrinsic ZBP1-MLKL-mediated ICD is also required for the synergetic antitumor effects of combination therapy. To further elucidate the impact of MLKL deficiency on the immune cell landscape under synergistic treatment, we quantified the proportions of $CD8^+$ T cells, DCs, $CD4^+$ T cells, and NK cells in tumors with CRISPR-Ctrl and $MLKL^{-/-}$ TUBO cells following combination therapy. The results revealed that $CD8^+$ T cell infiltration was compromised in MLKL-deficient tumors compared to control tumors treated with combination therapy (Figure S3E). Concomitantly, $MLKL^{-/-}$ tumors exhibited reduced DC infiltration and downregulated expression of CD80 on intratumoral DC following combination therapy (Figures S3F and S3G). In contrast, the infiltration of NK cells and $CD4^+$ T cells remained relatively unchanged (Figures S3H and S3I). These findings indicate that tumor cell-intrinsic MLKL is essential for enhancing tumor immunogenicity by facilitating $CD8^+$ T cell and DC recruitment in combination therapy. In addition, we found the combination of anti-HER2 mAb and 5AZA led to more pronounced activation of STAT1 than 5AZA treatment alone, and the inhibition of STAT1 abolished the ZBP1-dependent MLKL cascade in the context of combination therapy (Figure 3J), revealing that an increased expression of ZBP1 is more effectively induced by STAT1 signaling after combination treatments. Taken together, our data indicate that STAT1 promotes ZBP1 upregulation and subsequent MLKL activation in response to the combination treatment of 5AZA and anti-HER2 mAb.

Accumulation of Z-RNA promotes the activation of ZBP1 pathway after 5AZA treatment

It has been widely acknowledged that Z-RNA is detected by the Zα domain of ZBP1, but a recent study shows that Z-nucleic acid sensing is not essential for heat stress-triggered activation of ZBP1.[21,23,30] Thus, we assessed whether Z-RNA accumulation is necessary for ZBP1 activation induced by 5AZA treatment. A substantial increase of Z-RNA and dsRNA was observed in 5AZA-treated cells compared to the vehicle-treated group, and the addition of RNase mostly abolished Z-RNA formation (Figures 4A and S4A). Previous studies have demonstrated that 5AZA induces dsRNA formation by transcriptionally activating ERV and subsequently activating the MDA5/MAVS/IRF7 signaling pathway and that MAVS-induced type I IFN production is essential to induce ZBP1-dependent cell death.[25,31] We next sought to elucidate the contribution of the MDA5/MAVS/IRF7 pathway in ZBP1 pathway activation. Utilizing a lower dose of 5AZA in conjunction with anti-HER2 mAb, we observed upregulation of the MDA5/MAVS/IRF7 pathway (Figure S4B). Moreover, MAVS deficiency impaired STAT1-ZBP1 pathway activation following 5AZA treatment, suggesting that ZBP1 may not act as an independent mechanism in 5AZA therapy (Figure S4C). To further explore the interaction among Z-RNA, ZBP1, and MLKL, genetically modified 3T3 cells expressing either wild-type ZBP1 or ZBP1 mutants were utilized[23] (Figure 4B). Consistently, 5AZA induced both ZBP1-MLKL interaction and MLKL phosphorylation in 3T3 cells expressing these ZBP1 mutants, except for those expressing Flag-ΔZα2 and Flag-ΔRIP homotypic interaction motif A (RHIMA) (Figure 4C). However, proximity ligation assay (PLA) staining illustrated that Z-RNA specifically bound to the Zα2 domain of ZBP1 (Figure 4D). Thus, the Zα2 and RHIM A domains were both required for 5AZA-treated ZBP1-MLKL activation. In conclusion, these findings indicate that 5AZA activates ZBP1 through its Z-nucleic acid sensing and RHIM A domain for downstream activation.

It has been demonstrated that dsRNA originates from retroelements, and SETDB1 abrogation in bowel inflammation reactivates ERV, forming dsRNA that is sensed by ZBP1 to trigger necroptosis.[15,16] Thus, to determine the mechanism of Z-RNA accumulation following 5AZA treatment, we next explored whether SETDB1 was involved. In this study, we generated $SETDB1^{-/-}$ MC38 cells and observed significant Z-RNA accumulation in 5AZA-activated cells, $SETDB1^{-/-}$ cells, and $SETDB1^{-/-}$ cells treated with 5AZA (Figure 4E). In addition, SETDB1 expression was downregulated in both 5AZA monotherapy and combination therapy groups, and 5AZA treatment activated the ZBP1-MLKL necroptotic cascade, with SETDB1 deficiency further amplifying these effects (Figures 4F and 4G). However, SETDB1 deficiency had a minimal effect on the protein expression of the ZBP1 pathway, suggesting that SETDB1 loss predominantly affects Z-RNA formation rather than ZBP1 protein expression. To further elucidate whether 5AZA induces Z-RNA formation through the downregulation of SETDB1 expression,

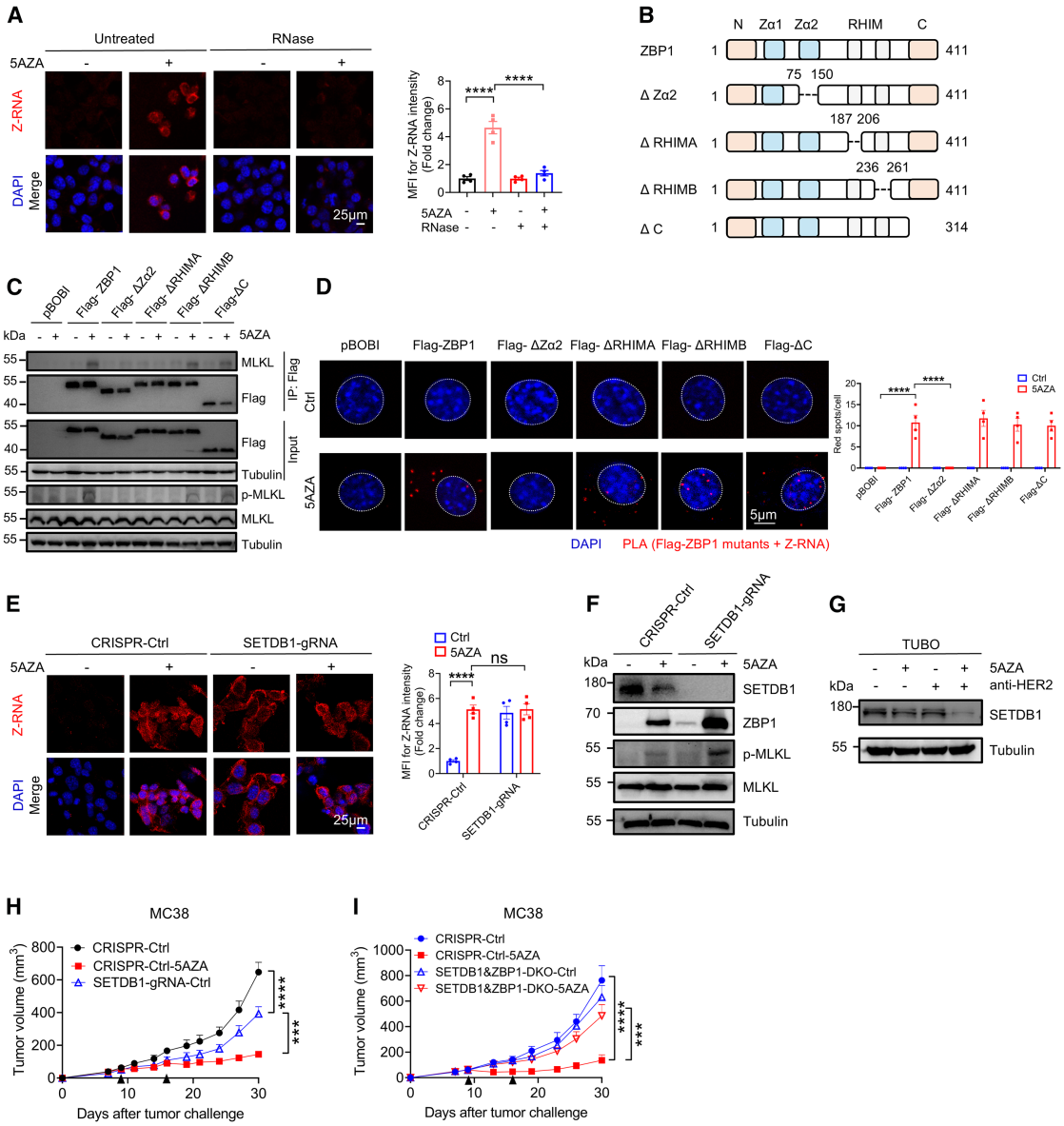

Figure 4. Accumulation of Z-RNA promotes the activation of ZBP1 pathway following 5AZA treatment

(A) Z-RNA accumulation in 5AZA-treated MC38 cells on day 5. Scale bars, 25 μm.

(B) Schematic representation of full-length ZBP1 or indicated mutants in ZBP1-deficient 3T3 cells.

(C) The interactions between MLKL and ZBP1 or its truncation mutants in 3T3 cells on day 5.

(D) The physical association between Z-RNA and ZBP1 or ZBP1 mutants in 3T3 cells on day 5. Scale bars, 5 μm.

(E) Z-RNA accumulation in SETDB1-deficient MC38 cells under 5AZA treatment on day 5. Scale bars, 25 μm.

(F) Protein expression of ZBP1-MLKL pathway in SETDB1-deficient MC38 cells after 5AZA treatment on day 5.

(G) SETDB1 expression after combination therapy in TUBO cells on day 5.

(H) Tumor growth of CRISPR-Ctrl, CRISPR-Ctrl-5AZA, and SETDB1$^{-/-}$ MC38 tumors. The black arrows indicate 5AZA therapy in the CRISPR-Ctrl-5AZA group (n = 5).

(I) Tumor growth of CRISPR-Ctrl and SETDB1&ZBP1$^{-/-}$ MC38 tumors after 5AZA treatment. The black arrows indicate 5AZA monotherapy (n = 5). Data are represented as means ± SEM. ***p < 0.001 and ****p < 0.0001 by one-way ANOVA in (A, D, and E) and two-way ANOVA in (H and I). See also Figure S4; Table S1.

we performed experiments involving SETDB1 overexpression in MC38 cells treated with 5AZA. Our results revealed that the overexpression of SETDB1 reversed the formation of Z-RNA, the activation of the ZBP1-MLKL pathway, and cell death caused by 5AZA treatment, demonstrating that 5AZA promotes Z-RNA formation by downregulating SETDB1 expression, which in turn activates the ZBP1-MLKL pathway (Figures S4D–S4F). Also, tumor volumes in the 5AZA treatment group demonstrated superior

tumor reduction compared to the SETDB1-ablation group (Figure 4H), revealing that Z-RNA formation is regulated by SETDB1 following 5AZA treatment. These data suggest that compared to SETDB1 ablation, 5AZA treatment generates multiple effects on tumor cells, including Z-RNA enrichment and ZBP1 upregulation.

To confirm whether ZBP1 is essential for SETDB1 impairment mediated necroptosis following 5AZA treatment, we genetically ablated both SETDB1 and ZBP1 or SETDB1 and MLKL in tumor cells. Deficiency of both SETDB1 and ZBP1 in 5AZA-induced cells partially restored necroptosis, and both SETDB1 and MLKL deficiency fully ablated necroptosis (Figures S4G and S4H). This result indicated that ZBP1 was essential for SETDB1 deficiency-mediated necroptosis following 5AZA treatment. Tumor growth studies indicated that while 5AZA therapy exerted robust antitumor effects, the combined deficiency of SETDB1 and ZBP1 largely abrogated the antitumor efficacy of 5AZA (Figure 4I). Furthermore, the effector function (IFN-γ) and the proliferation (Ki-67) of tumor-infiltrating $CD8^+$ T cell were impaired in SETDB1 and ZBP1 double-knockout tumors following 5AZA therapy (Figures S4I and S4J). The ELISPOT analysis also showed that impaired function of antigen-specific $CD8^+$ T cells contributed to the diminished therapeutic responses of SETDB1 and ZBP1 double-deficient tumors treated with 5AZA (Figures S4K and S4L). The above data indicate that ZBP1 is essential for the antitumor T cell responses elicited by SETDB1 deficiency following 5AZA treatment through Z-RNA-driven cell death signaling.

Increased Z-RNA gathering in senescent cells boosts ZBP1 activation under combination therapy of anti-HER2 and 5AZA

Senescence, a key factor in tumorigenesis, holds potential for therapeutic intervention.[32] SETDB1 expression decreases during aging, and the ERVs can be potential biomarkers to the aging process,[33,34] prompting us to investigate the relationship between cellular senescence, SETDB1, and Z-RNA in our experimental settings. Firstly, we determined whether senescence is associated with ZBP1-mediated innate immune sensing. As expected, using SA β-Gal staining (senescence-associated β1 galactosidase), we found that the combination therapy resulted in an increase in SA β-Gal^+ senescent cells as well as elevated mRNA levels of *p21* and *p27* in TUBO cells compared to either 5AZA or anti-HER2 mAb treatment alone (Figures 5A and 5B). Similarly, 5AZA treatment alone also resulted in an accumulation of SA β-Gal^+ senescent cells in MC38 and E0771 tumor cells (Figures S5A and S5B). These data uncover that the combination of anti-HER2 mAb and 5AZA induces an enhanced cellular senescence compared to the single treatment.

Moreover, we found no changes in SA-β-Gal-positive cells numbers between ZBP1-deficient cells and CRISPR-Ctrl cells after combination treatments, indicating that ZBP1 does not regulate cell senescence in this setting (Figure S5C). To determine whether cellular senescence was associated with Z-RNA formation, we performed co-staining of Z-RNA and SPiDER-β-Gal.[34] The combination treatment displayed more co-localization of Z-RNA and SPiDER-β-Gal, suggesting preferential accumulation of Z-RNA in senescent cells (Figure 5C). Besides, we also observed an increase in the percentage of β-gal-positive cells and Z-RNA formation over the course of the combination treatment, with a progressive rise from day 0 to day 5 (S5D-E), indicating that Z-RNA accumulates during senescence. To further investigate whether ZBP1 activation induced by the combination of 5AZA and anti-HER2 mAb in senescent cells, we separate $SPiDER^+$ and $SPiDER^-$ cells by flow sorting following combination treatment. $SPiDER^+$ cells showed elevated ZBP1 and *p*-MLKL expression compared with $SPiDER^-$ cells under combination treatment (Figure 5D). We next utilize senolysis therapy to pharmacologically eliminate senescent cells. Given the elevated expression of *Bcl-2* family in senescent cancer cells (Figure S5F), we employed ABT-263, a potent *Bcl-2* expression inhibitor, to selectively target and eliminate senescent cells.[35–37] Our data showed that ABT-263 selectively targeted senescent cells under combination therapy (Figure 5E). The addition of ABT-263 reversed ZBP1 expression and Z-RNA formation induced by the combination treatment in TUBO cells (Figures 5F and 5G). These findings indicate that increased Z-RNA accumulating during senescence boosts ZBP1 activation under combination therapy.

Next, we sought to further elucidate the interplay between SETDB1 and cellular senescence following synergistic treatment. We found ABT-263 selectively targeted senescent cells under combination therapy, resulting in a partial recovery of SETDB1 expression (Figure 5H). To evaluate the impact of SETDB1 loss on the senescence phenotype, we next generated a SETDB1-deficient TUBO cell line and treated it with anti-HER2 mAb and 5AZA. However, neither SA-β-Gal staining nor reverse transcription-polymerase chain reaction (RT-PCR) analysis of *p21* and *p27* showed significant alterations in the SETDB1-knockout cells post-treatment, suggesting that SETDB1-deficient cells still undergo senescence and that SETDB1 loss does not impair senescence induction following combination treatment (Figures 5I and S5G). Moreover, the addition of ABT-263 showed no effects on Z-RNA accumulation and ZBP1 expression in SETDB1-knockout cells (Figures 5J and 5K). It suggested that not all Z-RNA-positive cells in the SETDB1-KO group were senescent and therefore partially resistant to ABT-263-mediated clearance. These findings indicate that combination treatment leads to cellular senescence accompanied by a decrease of SETDB1 expression, which synergistically promotes Z-RNA accumulation and boosts ZBP1 activation.

Additionally, considering that HER2 disrupts STING signaling, thereby suppressing antitumor immunity,[5] we also investigate whether necroptosis is triggered by combination therapy through the engagement of STING pathway or senescence. We found that the STING inhibitor H151 did not affect cellular senescence and Z-RNA formation but decreased the activation of ZBP1 and MLKL phosphorylation (Figures S5H–S5J), indicating that these two mechanisms are complementary to trigger necroptosis after 5AZA and anti-HER2 combination treatment.

DISCUSSION

Understanding the immune-related mechanisms of DNA-demethylating agents aids in the design of effective anti-HER2

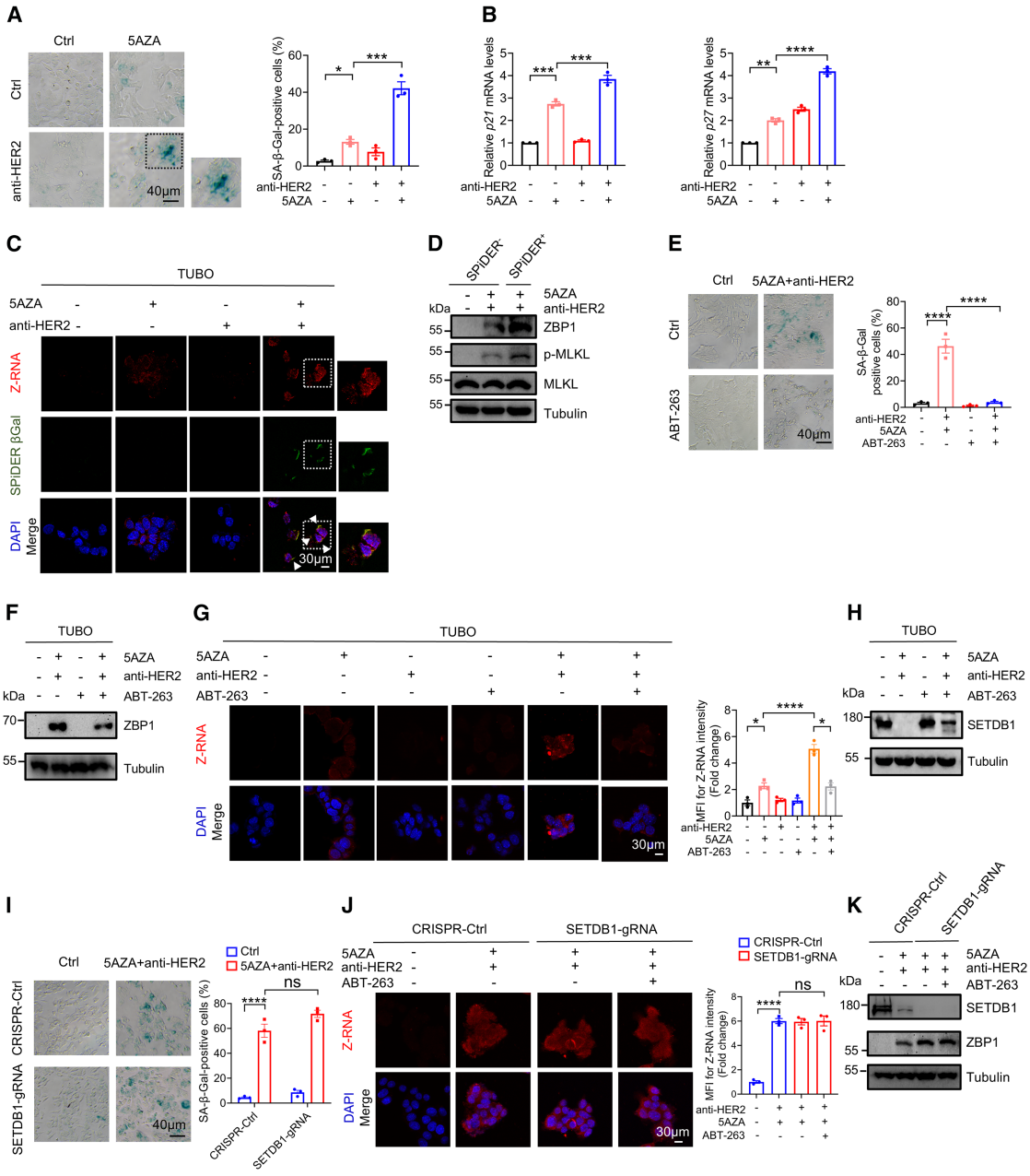

Figure 5. Increased Z-RNA gathering in senescent tumor cells boosts ZBP1 activation under combination therapy of 5AZA and anti-HER2 mAb

(A and B) Combination therapy with anti-HER2 mAb and 5AZA induced cellular senescence in TUBO cells on day 5. Scale bars, 40 μm.

(C) Immunofluorescence of SPiDER βGal and Z-RNA in TUBO cells after combination therapy on day 5. The white arrows indicate double-positive cells. Scale bars, 30 μm.

(D) Expression levels of ZBP-MLKL pathway in SPiDER^{+} and SPiDER^{-} TUBO cells under synergized therapy on day 5.

(E) SA-β-gal staining after pharmacologic elimination of senescent cells and combination therapy in TUBO cells on day 5. Scale bars, 40 μm.

(F) Elimination of senescent cells decreased ZBP1 activation in TUBO cells on day 5.

(G) Decreased Z-RNA accumulation in senescence-depleted cells in synergized treatment in TUBO cells on day 5. Scale bars, 30 μm.

(H) Elimination of senescent cells partially restored SETDB1 expression after combination therapy in TUBO cells on day 5.

(I) SA-β-gal staining of SETDB1-abrogating TUBO cells after combination treatments on day 5. Scale bars, 40 μm.

(J) Z-RNA accumulation in SETDB1-deficient TUBO cells after combination treatment of ABT-263, 5AZA, and anti-HER2 mAb on day 5. Scale bars, 30 μm.

(K) Expression of ZBP1 in SETDB1-deficient TUBO cells after combination treatment of ABT-263, 5AZA, and anti-HER2 mAb on day 5. Data are represented as means ± SEM. *$p < 0.05$, **$p < 0.01$, ***$p < 0.001$, and ****$p < 0.0001$ by one-way ANOVA in (A, B, E, G, I, and J). See also Figure S5; Table S1.

antibody therapy. In this study, we provide a rationale that the epigenetic agent 5AZA enhances anti-HER2 targeted therapy by promoting ZBP1-mediated tumor immunogenicity. Furthermore, the increased accumulation of Z-RNA during senescence promotes ZBP1 activation. Our findings support the pivotal role of ZBP1-mediated tumor immunogenicity in bridging tumor stress responses and antitumor adaptive immunity following the combination of anti-HER2 therapy and 5AZA treatment.

The DNMT inhibitor 5AZA has recently elucidated its integral role in solid tumors.[25,38] On the one hand, low-dose 5AZA stimulates antitumor responses by generating dsRNA and depleting ADAR1, which is an RNA-editing enzyme, potentiates viral mimicry responses.[17,25] On the other hand, intraperitoneal administration of 5AZA potently enhances $CD8^+$ T cells infiltration and cytolytic activity in tumors, substantiating its use as an immunotherapeutic agent.[39] Still, the mechanisms underlying the action of 5AZA in solid tumor are not fully established. To elucidate the role of tumor-intrinsic immunogenicity, intratumoral 5AZA and intraperitoneal anti-HER2 mAb administration were conducted. This approach allowed us to separate the effect of 5AZA on tumor cell activity from that driven by the host immune responses.[40,41] Since anti-HER2 treatment did not induce ZBP1 expression, our subsequent investigations focused on both 5AZA monotherapy and combination treatment to further investigate whether the tumor cell-intrinsic ZBP1 exerts any effects on tumor-infiltrating $CD8^+$ T cells. Notably, TUBO tumors exhibit relatively low immunogenicity, which may limit the ability of 5AZA monotherapy to elicit robust antitumor immune responses. Our previous study has demonstrated that 5AZA monotherapy activates ZBP1 in MC38 cells, a mouse colon adenocarcinoma cell line with stronger immunogenicity.[12] Thus, to further investigate the potential impact of tumor cell-intrinsic ZBP1 on $CD8^+$ T cell response, MC38 was selected because of its robust immunogenicity and sensitivity to T cell-mediated responses, allowing us to assess $CD8^+$ T cell functionality *in vivo*.

ZBP1 pathway activation is an underappreciated component of cancer immune responses, and ADAR1 suppresses endogenous Z-RNA and inhibits ZBP1-mediated necroptosis.[8] In autoinflammatory diseases, retroelement-derived Z-RNA activates ZBP1 in mice with ADAR1 Zα mutation.[42–44] In cardiac damage responses, ZBP1 stabilizes Z-DNA from mitochondrial instability and engages cGAS in a DNA- and RHIM-dependent manner.[45] Our previous research demonstrated that the ZBP1-MLKL pathway supports $CD8^+$ T cell effector function in irradiated tumors.[12] Yet, it remains unknown whether Z-RNA sensing contributes to the sensitivity of anti-HER2 treatment. Tumor regression and *in vivo* $CD8^+$ T cell antitumor effects of combination therapy were largely dependent on tumor-intrinsic ZBP1 activation. Additionally, we observed robust Z-RNA enrichment and ZBP1 generation in response to 5AZA and combination therapies, but not in anti-HER2 treatment alone. This suggests that ZBP1 pathway activation is not a general mechanism of anti-HER2 therapy.

Viral mimicry is an antiviral state induced by endogenous RNA or DNA derived from retrotransposon transcripts, rather than by exogenous viral infections.[46] Epigenetic therapies, particularly DNA-demethylating agents, are central to eliciting viral mimicry responses through the induction of ERV-derived dsRNA accumulation in cancer treatment.[25] We propose that the Z-RNA/ZBP1 pathway is activated under 5-AZA treatment and synergistic therapy. However, it remains unclear whether ERVs are the sole source of Z-RNA during viral mimicry or if mitochondrial RNA also plays a role. In scenarios of viral infection, ZBP1 activation requires both the Zα and RHIM domains.[30,47] However, Z-nucleic acid sensing is not mandatory for ZBP1 activation in heat stress, suggesting that there may be multiple mechanisms for ZBP1 activation.[23] We demonstrated that Z-RNA was bound to the Zα2 domain of ZBP1, and both the Zα2 and RHIM A domains were essential for ZBP1-MLKL activation. This suggests that tumor endogenous ZBP1-mediated ICD triggers antitumor immune responses after 5AZA treatment alone or combination treatment with anti-HER2 mAb. However, the activation of ZBP1 leads to cell death but also induces inflammation independent of cell death. We could not rule out the effect of ZBP1-induced inflammation in our settings.

Senescence, a key factor in tumorigenesis, holds potential for therapeutic intervention.[32] Recent studies have revealed the essential role of cytosolic DNA and RNA sensing in senescence.[5,48,49] HER2 regulates senescence-associated inflammation by disturbing the STING pathway and RIG-I signaling.[5,49] In systemic lupus erythematosus, MAVS-IFN-β loop instigates cellular senescence.[50] Aging-related necroptosis impairs hematopoietic stem cells (HSCs), and abrogation of necroptosis improves the self-renewal capacity of HSCs.[51] Although the role of DNA sensing and RIG-MAVS pathways in senescence are well established, the interplay between senescence and the ZBP1 pathway remains underexplored. In this study, we observed increased SA-β-Gal staining in the combination treatment group, while ZBP1 abrogation did not affect senescence. Combination treatment displayed cellular co-location of Z-RNA and SPiDER-β-Gal, suggesting that senescent tumor cells provide a harbor for optimal Z-RNA/ZBP1 sensing. Senolytic therapies targeting TIMP1-loss senescent tumor cells have been shown to effectively reduce prostate cancer metastasis.[37] Additionally, combining arginine inhibition, GCN2 hindrance, and senolytic agents induces hepatocellular cell death.[52] Above all, the increased Z-RNA formation during senescence process drives ZBP1 activation, positioning senescence as a key contributor to tumor immunogenicity.

SETDB1 plays a pivotal role in maintaining heterochromatin integrity and silencing ERV. Loss of SETDB1 significantly upregulates ERV expression in radiation-treated cells, leading to the activation of MDA5/MAVS-mediated type I interferon responses.[15,16,53] Furthermore, SETDB1 abrogation reactivates ERV, resulting in the formation of dsRNA sensed by ZBP1 for necroptosis.[16] Retrotransposons de-repression during senescence triggers type I interferon responses, highlighting their significance in cellular senescence.[54,55] ERV has been identified as a potential biomarker and driver of aging, prompting further investigation into the relationship between cellular senescence, SETDB1, and Z-RNA.[34] Although our *in vivo* studies using SETDB1 and ZBP1 knockout models under 5AZA monotherapy indicated that the ZBP1 pathway was the primary driver of the observed tumor immunogenicity, the results that deficiency of both SETDB1 and ZBP1 in 5AZA-induced cell partially restored necroptosis and both SETDB1

and MLKL deficiency fully ablated necroptosis suggest that other factors may also contribute to necroptosis. Senescent cells secrete a senescence-associated secretory phenotype (SASP), which includes factors such as TNF, p21, and p27, and enhance mitochondrial ROS generation.[56] It is possible that TNF induces MLKL phosphorylation, thereby promoting necroptosis,[57] or that mitochondrial ROS also enhances MLKL-dependent necroptosis.[58]

In our study, possible links between cellular senescence and SETDB1 expression are elucidated. We found that cellular senescence was accompanied by a decrease in SETDB1 expression after combination therapy, which is consistent with previous reports that SETDB1 reduces in an accelerated aging disease and that deletion of SETDB1 induces senescence-like changes in macrophages.[33,59] However, our results showed that both 5AZA alone and in combination with anti-HER2 antibody induced cell senescence and that the removal of the senescent cell led to a partial recovery of SETDB1 expression, indicating that there are other potential mechanisms mediating SETDB1 downregulation after combination treatment. Low-dose 5AZA specifically decreases gene body methylation and downregulates oncogene expression, which is also linked to changes in histone marks and chromatin accessibility.[38] Also, lineage-specific gene body DNA methylation coincides with SETDB1 recruitment.[60] Thus, further investigation is needed to clarify the molecular mechanisms underlying SETDB1 downregulation.

Our study also suggests that during 5AZA monotherapy or combination treatment, the cGAS-STING pathway contributes to ZBP1 expression and downstream MLKL phosphorylation but has no significant impact on cellular senescence and Z-RNA formation. Notably, the elimination of senescent cells with ABT-263 both inhibited ZBP1 expression and Z-RNA formation induced by combination treatment. We have previously reported a positive feedback loop between ZBP1-MLKL necroptotic cascade and cGAS-STING signaling in irradiated tumors, and there are known links among the ZBP1-MLKL, cGAS-STING, and type I interferon pathways.[12,61] Considering that STAT1 is a downstream factor of the cGAS-STING type I interferon pathway and mediates ZBP1 activation in our study, it is possible that the STING signaling pathway promotes ICD by upregulating ZBP1 and exerts complementary effects with cellular senescence in this setting.

In this study, multiple cell lines were employed to demonstrate that the ZBP1 pathway enhances tumor immunogenicity following 5-AZA monotherapy or combination treatment. The consistent activation of ZBP1 across various cell types suggests a conserved mechanism; however, we cannot rule out the possibility of alternative mechanisms under specific conditions or in certain cell lines. To investigate the mechanism of ZBP1 activation, we utilized the mouse fibroblast cell line 3T3, a well-established model in tumorigenesis research that recapitulates key molecular pathways in cancer cells.[62–64] While the fibroblast model identified the Zα2 and RHIM A domains as essential for ZBP1–MLKL activation, it remains to be determined whether this mechanism is applicable in other contexts, particularly in epithelial cancers.

In conclusion, we validate the therapeutic potential of combining epigenetic intervention with anti-HER2 mAb, which primarily depends on ZBP1-mediated tumor immunogenicity and boosts antitumor $CD8^+$ T cell responses. The increased accumulation of Z-RNA during senescence promotes ZBP1 activation, positioning senescence as a key contributing factor in tumor immunogenicity. These findings suggest that Z-RNA sensing is a switch linking cellular senescence with intrinsic tumor immunogenicity, offering insights of a strategy for overcoming resistance in anti-HER2 therapy.

Limitations of the study

Although our work highlights the promise of combining 5AZA with anti-HER2 mAb to induce Z-RNA/ZBP1 activation in $HER2^+$ BRCA, it still remains unknown whether these synergistic effects are broadly applicable across different cancer types. The two cell lines TUBO and MC38 were employed to address specific research questions. However, we did not consolidate the conclusion by employing $HER2^+$ BRCA cells following 5AZA therapy. The inherent differences and varying immunogenicity between these cell lines may limit the generalizability of our findings. Also, the use of fibroblast model to elucidate mechanistic details is a limitation considering the possible impact on carcinomas (epithelial cell-derived cancers). Whether ZBP1 can be a clinical biomarker of tumor prognosis in patients with anti-HER2 therapy warrants further investigations, as well as whether the identification of tumor cell-intrinsic ZBP1 expression is critical for successful combination therapies. Moreover, whether senescence influences SETDB1 in other tumor contexts and whether senescent cells attract more immune cells in this setting are both in dispute and need further investigation. Lastly, whether anti-HER2 ADC (anti-HER2 antibody conjugates with low-dose 5AZA) is a promising therapeutic strategy that needs further investigation.

RESOURCE AVAILABILITY

Lead contact

Further information and requests for resources and reagents should be directed to and will be fulfilled by the lead contact, Liufu Deng (dengliufu@sjtu.edu.cn).

Materials availability

All unique/stable reagents generated in this study are available from the lead contact with a completed materials transfer agreement.

Data and code availability

- All data reported in this paper will be shared by the lead contact upon request.
- This paper does not report original code.
- Any additional information required to reanalyze the data reported in this paper is available from the lead contact upon request.

ACKNOWLEDGMENTS

The authors thank Prof. Ben Lu at the Central South University, Hunan, China, for kindly providing plasmids encoding ZBP1 truncated mutations. This work was supported by National Natural Science Foundation of China (NSFC) grants 82350115, 81771682, and 82071741 to L.D.; 32470962 to L.L.; National Thousand Youth Talents Program to L.D.; Science and Technology Commission of Shanghai Municipality 16JC1406000 to L.D.; and Fundamental Research Funds for the Central Universities and Interdisciplinary Program of Shanghai Jiao Tong University YG2021ZD03 to L.D. Graphical abstract was created with BioRender.com.

AUTHOR CONTRIBUTIONS

Q.W. and Z.W. performed the experiments and wrote original draft. Y.Y., C.Y., H.D., X.Z., S.X., L.W., X.H., X.Y., and L.L. contributed to part of the *in vivo* experiments. H.D., X.Z., S.X., L.W., X.H., and X.Y. aided in the experiments of flow cytometry assay. Q.W. and Z.W. analyzed the data. L.L. and L.D. revised the manuscript and conceived and supervised all experiments.

DECLARATION OF INTERESTS

L.D. and Q.W. have filed a patent application related to this project.

STAR★METHODS

Detailed methods are provided in the online version of this paper and include the following:

- KEY RESOURCES TABLE
- EXPERIMENTAL MODEL AND STUDY PARTICIPANT DETAILS
  - Mice
  - Cells and cell culture
- METHOD DETAILS
  - Plasmids construction and transfection
  - Pharmacological treatment
  - *In vivo* tumor models
  - Flow cytometry
  - ELISPOT assay
  - Prediction of transcription factor of ZBP1
  - Prognostic analysis of ZBP1 in $HER2^{+}$ BRCA
  - Western blot and co-immunoprecipitation assay
  - RNA purification and RT-PCR
  - Immunofluorescence imaging
  - *In situ* proximity ligation assay (PLA)
  - Senescence-associated β1 galactosidase (SA-β-gal)
  - Cell isolation by flow cytometry
  - Cell growth rate assay
- QUANTIFICATION AND STATISTICAL ANALYSIS

SUPPLEMENTAL INFORMATION

Supplemental information can be found online at https://doi.org/10.1016/j.celrep.2025.116314.

Received: January 26, 2025
Revised: July 8, 2025
Accepted: August 28, 2025

REFERENCES

1. Park, S., Jiang, Z., Mortenson, E.D., Deng, L., Radkevich-Brown, O., Yang, X., Sattar, H., Wang, Y., Brown, N.K., Greene, M., et al. (2010). The therapeutic effect of anti-HER2/neu antibody depends on both innate and adaptive immunity. Cancer Cell *18*, 160–170. https://doi.org/10.1016/j.ccr.2010.06.014.
2. Rimawi, M.F., Schiff, R., and Osborne, C.K. (2015). Targeting HER2 for the treatment of breast cancer. Annu. Rev. Med. *66*, 111–128. https://doi.org/10.1146/annurev-med-042513-015127.
3. Todorović-Raković, N., and Milovanović, J. (2013). Interleukin-8 in breast cancer progression. J. Interferon Cytokine Res. *33*, 563–570. https://doi.org/10.1089/jir.2013.0023.
4. Paplomata, E., and O'Regan, R. (2014). The PI3K/AKT/mTOR pathway in breast cancer: targets, trials and biomarkers. Ther. Adv. Med. Oncol. *6*, 154–166. https://doi.org/10.1177/1758834014530023.
5. Wu, S., Zhang, Q., Zhang, F., Meng, F., Liu, S., Zhou, R., Wu, Q., Li, X., Shen, L., Huang, J., et al. (2019). HER2 recruits AKT1 to disrupt STING signalling and suppress antiviral defence and antitumour immunity. Nat. Cell Biol. *21*, 1027–1040. https://doi.org/10.1038/s41556-019-0352-z.
6. Jhunjhunwala, S., Hammer, C., and Delamarre, L. (2021). Antigen presentation in cancer: insights into tumour immunogenicity and immune evasion. Nat. Rev. Cancer *21*, 298–312. https://doi.org/10.1038/s41568-021-00339-z.
7. Schadt, L., Sparano, C., Schweiger, N.A., Silina, K., Cecconi, V., Lucchiari, G., Yagita, H., Guggisberg, E., Saba, S., Nascakova, Z., et al. (2019). Cancer-Cell-Intrinsic cGAS Expression Mediates Tumor Immunogenicity. Cell Rep. *29*, 1236–1248.e7. https://doi.org/10.1016/j.celrep.2019.09.065.
8. Zhang, T., Yin, C., Fedorov, A., Qiao, L., Bao, H., Beknazarov, N., Wang, S., Gautam, A., Williams, R.M., Crawford, J.C., et al. (2022). ADAR1 masks the cancer immunotherapeutic promise of ZBP1-driven necroptosis. Nature *606*, 594–602. https://doi.org/10.1038/s41586-022-04753-7.
9. Galluzzi, L., Vitale, I., Aaronson, S.A., Abrams, J.M., Adam, D., Agostinis, P., Alnemri, E.S., Altucci, L., Amelio, I., Andrews, D.W., et al. (2018). Molecular mechanisms of cell death: recommendations of the Nomenclature Committee on Cell Death 2018. Cell Death Differ. *25*, 486–541. https://doi.org/10.1038/s41418-017-0012-4.
10. Snyder, A.G., Hubbard, N.W., Messmer, M.N., Kofman, S.B., Hagan, C.E., Orozco, S.L., Chiang, K., Daniels, B.P., Baker, D., and Oberst, A. (2019). Intratumoral activation of the necroptotic pathway components RIPK1 and RIPK3 potentiates antitumor immunity. Sci. Immunol. *4*, eaaw2004. https://doi.org/10.1126/sciimmunol.aaw2004.
11. Ahmed, A., and Tait, S.W.G. (2020). Targeting immunogenic cell death in cancer. Mol. Oncol. *14*, 2994–3006. https://doi.org/10.1002/1878-0261.12851.
12. Yang, Y., Wu, M., Cao, D., Yang, C., Jin, J., Wu, L., Hong, X., Li, W., Lu, L., Li, J., et al. (2021). ZBP1-MLKL necroptotic signaling potentiates radiation-induced antitumor immunity via intratumoral STING pathway activation. Sci. Adv. *7*, eabf6290. https://doi.org/10.1126/sciadv.abf6290.
13. Marin, I., Boix, O., Garcia-Garijo, A., Sirois, I., Caballe, A., Zarzuela, E., Ruano, I., Attolini, C.S.O., Prats, N., López-Domínguez, J.A., et al. (2023). Cellular Senescence Is Immunogenic and Promotes Antitumor Immunity. Cancer Discov. *13*, 410–431. https://doi.org/10.1158/2159-8290.Cd-22-0523.
14. Chibaya, L., Murphy, K.C., DeMarco, K.D., Gopalan, S., Liu, H., Parikh, C.N., Lopez-Diaz, Y., Faulkner, M., Li, J., Morris, J.P., 4th, et al. (2023). EZH2 inhibition remodels the inflammatory senescence-associated secretory phenotype to potentiate pancreatic cancer immune surveillance. Nat. Cancer *4*, 872–892. https://doi.org/10.1038/s43018-023-00553-8.
15. Jiao, H., Wachsmuth, L., Kumari, S., Schwarzer, R., Lin, J., Eren, R.O., Fisher, A., Lane, R., Young, G.R., Kassiotis, G., et al. (2020). Z-nucleic-acid sensing triggers ZBP1-dependent necroptosis and inflammation. Nature *580*, 391–395. https://doi.org/10.1038/s41586-020-2129-8.
16. Wang, R., Li, H., Wu, J., Cai, Z.Y., Li, B., Ni, H., Qiu, X., Chen, H., Liu, W., Yang, Z.H., et al. (2020). Gut stem cell necroptosis by genome instability triggers bowel inflammation. Nature *580*, 386–390. https://doi.org/10.1038/s41586-020-2127-x.
17. Mehdipour, P., Marhon, S.A., Ettayebi, I., Chakravarthy, A., Hosseini, A., Wang, Y., de Castro, F.A., Loo Yau, H., Ishak, C., Abelson, S., et al. (2020). Epigenetic therapy induces transcription of inverted SINEs and ADAR1 dependency. Nature *588*, 169–173. https://doi.org/10.1038/s41586-020-2844-1.
18. Tang, Q., Rigby, R.E., Young, G.R., Hvidt, A.K., Davis, T., Tan, T.K., Bridgeman, A., Townsend, A.R., Kassiotis, G., and Rehwinkel, J. (2021). Adenosine-to-inosine editing of endogenous Z-form RNA by the deaminase ADAR1 prevents spontaneous MAVS-dependent type I interferon responses. Immunity *54*, 1961–1975.e5. https://doi.org/10.1016/j.immuni.2021.08.011.
19. Athanasiadis, A. (2012). Zalpha-domains: at the intersection between RNA editing and innate immunity. Semin. Cell Dev. Biol. *23*, 275–280. https://doi.org/10.1016/j.semcdb.2011.11.001.

20. Kim, S.H., Lim, S.H., Lee, A.R., Kwon, D.H., Song, H.K., Lee, J.H., Cho, M., Johner, A., Lee, N.K., and Hong, S.C. (2018). Unveiling the pathway to Z-DNA in the protein-induced B-Z transition. Nucleic Acids Res. *46*, 4129–4137. https://doi.org/10.1093/nar/gky200.

21. Li, S., Zhang, Y., Guan, Z., Ye, M., Li, H., You, M., Zhou, Z., Zhang, C., Zhang, F., Lu, B., et al. (2023). SARS-CoV-2 Z-RNA activates the ZBP1-RIPK3 pathway to promote virus-induced inflammatory responses. Cell Res. *33*, 201–214. https://doi.org/10.1038/s41422-022-00775-y.

22. Yang, T., Wang, G., Zhang, M., Hu, X., Li, Q., Yun, F., Xing, Y., Song, X., Zhang, H., Hu, G., and Qian, Y. (2023). Triggering endogenous Z-RNA sensing for anti-tumor therapy through ZBP1-dependent necroptosis. Cell Rep. *42*, 113377. https://doi.org/10.1016/j.celrep.2023.113377.

23. Yuan, F., Cai, J., Wu, J., Tang, Y., Zhao, K., Liang, F., Li, F., Yang, X., He, Z., Billiar, T.R., et al. (2022). Z-DNA binding protein 1 promotes heatstroke-induced cell death. Science *376*, 609–615. https://doi.org/10.1126/science.abg5251.

24. Baik, J.Y., Liu, Z., Jiao, D., Kwon, H.J., Yan, J., Kadigamuwa, C., Choe, M., Lake, R., Kruhlak, M., Tandon, M., et al. (2021). ZBP1 not RIPK1 mediates tumor necroptosis in breast cancer. Nat. Commun. *12*, 2666. https://doi.org/10.1038/s41467-021-23004-3.

25. Roulois, D., Loo Yau, H., Singhania, R., Wang, Y., Danesh, A., Shen, S.Y., Han, H., Liang, G., Jones, P.A., Pugh, T.J., et al. (2015). DNA-Demethylating Agents Target Colorectal Cancer Cells by Inducing Viral Mimicry by Endogenous Transcripts. Cell *162*, 961–973. https://doi.org/10.1016/j.cell.2015.07.056.

26. Rovero, S., Amici, A., Di Carlo, E., Bei, R., Nanni, P., Quaglino, E., Porcedda, P., Boggio, K., Smorlesi, A., Lollini, P.L., et al. (2000). DNA vaccination against rat her-2/Neu p185 more effectively inhibits carcinogenesis than transplantable carcinomas in transgenic BALB/c mice. J. Immunol. *165*, 5133–5142. https://doi.org/10.4049/jimmunol.165.9.5133.

27. Zhu, S., Luo, Y., Li, K., Mei, C., Wang, Y., Jiang, L., Wang, W., Zhang, Q., Yang, W., Lang, W., et al. (2024). RIPK3 deficiency blocks R-2-hydroxyglutarate-induced necroptosis in IDH-mutated AML cells. Sci. Adv. *10*, eadi1782. https://doi.org/10.1126/sciadv.adi1782.

28. Kuriakose, T., and Kanneganti, T.D. (2018). ZBP1: Innate Sensor Regulating Cell Death and Inflammation. Trends Immunol. *39*, 123–134. https://doi.org/10.1016/j.it.2017.11.002.

29. Frank, D.A., Mahajan, S., and Ritz, J. (1999). Fludarabine-induced immunosuppression is associated with inhibition of STAT1 signaling. Nat. Med. *5*, 444–447. https://doi.org/10.1038/7445.

30. Zhang, T., Yin, C., Boyd, D.F., Quarato, G., Ingram, J.P., Shubina, M., Ragan, K.B., Ishizuka, T., Crawford, J.C., Tummers, B., et al. (2020). Influenza Virus Z-RNAs Induce ZBP1-Mediated Necroptosis. Cell *180*, 1115–1129.e13. https://doi.org/10.1016/j.cell.2020.02.050.

31. Kesavardhana, S., Kuriakose, T., Guy, C.S., Samir, P., Malireddi, R.K.S., Mishra, A., and Kanneganti, T.D. (2017). ZBP1/DAI ubiquitination and sensing of influenza vRNPs activate programmed cell death. J. Exp. Med. *214*, 2217–2229. https://doi.org/10.1084/jem.20170550.

32. Wang, L., Lankhorst, L., and Bernards, R. (2022). Exploiting senescence for the treatment of cancer. Nat. Rev. Cancer *22*, 340–355. https://doi.org/10.1038/s41568-022-00450-9.

33. Lee, J.H., Demarest, T.G., Babbar, M., Kim, E.W., Okur, M.N., De, S., Croteau, D.L., and Bohr, V.A. (2019). Cockayne syndrome group B deficiency reduces H3K9me3 chromatin remodeler SETDB1 and exacerbates cellular aging. Nucleic Acids Res. *47*, 8548–8562. https://doi.org/10.1093/nar/gkz568.

34. Liu, X., Liu, Z., Wu, Z., Ren, J., Fan, Y., Sun, L., Cao, G., Niu, Y., Zhang, B., Ji, Q., et al. (2023). Resurrection of endogenous retroviruses during aging reinforces senescence. Cell *186*, 287–304.e26. https://doi.org/10.1016/j.cell.2022.12.017.

35. Mylonas, K.J., O'Sullivan, E.D., Humphries, D., Baird, D.P., Docherty, M.H., Neely, S.A., Krimpenfort, P.J., Melk, A., Schmitt, R., Ferreira-Gonzalez, S., et al. (2021). Cellular senescence inhibits renal regeneration after injury in mice, with senolytic treatment promoting repair. Sci. Transl. Med. *13*, eabb0203. https://doi.org/10.1126/scitranslmed.abb0203.

36. Prieto, L.I., Sturmlechner, I., Graves, S.I., Zhang, C., Goplen, N.P., Yi, E.S., Sun, J., Li, H., and Baker, D.J. (2023). Senescent alveolar macrophages promote early-stage lung tumorigenesis. Cancer Cell *41*, 1261–1275.e6. https://doi.org/10.1016/j.ccell.2023.05.006.

37. Guccini, I., Revandkar, A., D'Ambrosio, M., Colucci, M., Pasquini, E., Mosole, S., Troiani, M., Brina, D., Sheibani-Tezerji, R., Elia, A.R., et al. (2021). Senescence Reprogramming by TIMP1 Deficiency Promotes Prostate Cancer Metastasis. Cancer Cell *39*, 68–82.e69. https://doi.org/10.1016/j.ccell.2020.10.012.

38. Yang, X., Han, H., De Carvalho, D.D., Lay, F.D., Jones, P.A., and Liang, G. (2014). Gene body methylation can alter gene expression and is a therapeutic target in cancer. Cancer Cell *26*, 577–590. https://doi.org/10.1016/j.ccr.2014.07.028.

39. Loo Yau, H., Bell, E., Ettayebi, I., de Almeida, F.C., Boukhaled, G.M., Shen, S.Y., Allard, D., Morancho, B., Marhon, S.A., Ishak, C.A., et al. (2021). DNA hypomethylating agents increase activation and cytolytic activity of CD8(+) T cells. Mol. Cell *81*, 1469–1483.e8. https://doi.org/10.1016/j.molcel.2021.01.038.

40. Falahat, R., Berglund, A., Perez-Villarroel, P., Putney, R.M., Hamaidi, I., Kim, S., Pilon-Thomas, S., Barber, G.N., and Mulé, J.J. (2023). Epigenetic state determines the in vivo efficacy of STING agonist therapy. Nat. Commun. *14*, 1573. https://doi.org/10.1038/s41467-023-37217-1.

41. Huang, C., Tian, Y., Peng, R., Zhang, C., Wang, D., Han, S., Jiao, C., Wang, X., Zhang, H., Wang, Y., and Li, X. (2015). Association of downregulation of WWOX with poor prognosis in patients with intrahepatic cholangiocarcinoma after curative resection. J. Gastroenterol. Hepatol. *30*, 421–433. https://doi.org/10.1111/jgh.12722.

42. Jiao, H., Wachsmuth, L., Wolf, S., Lohmann, J., Nagata, M., Kaya, G.G., Oikonomou, N., Kondylis, V., Rogg, M., Diebold, M., et al. (2022). ADAR1 averts fatal type I interferon induction by ZBP1. Nature *607*, 776–783. https://doi.org/10.1038/s41586-022-04878-9.

43. de Reuver, R., Verdonck, S., Dierick, E., Nemegeer, J., Hessmann, E., Ahmad, S., Jans, M., Blancke, G., Van Nieuwerburgh, F., Botzki, A., et al. (2022). ADAR1 prevents autoinflammation by suppressing spontaneous ZBP1 activation. Nature *607*, 784–789. https://doi.org/10.1038/s41586-022-04974-w.

44. Hubbard, N.W., Ames, J.M., Maurano, M., Chu, L.H., Somfleth, K.Y., Gokhale, N.S., Werner, M., Snyder, J.M., Lichauco, K., Savan, R., et al. (2022). ADAR1 mutation causes ZBP1-dependent immunopathology. Nature *607*, 769–775. https://doi.org/10.1038/s41586-022-04896-7.

45. Lei, Y., VanPortfliet, J.J., Chen, Y.F., Bryant, J.D., Li, Y., Fails, D., Torres-Odio, S., Ragan, K.B., Deng, J., Mohan, A., et al. (2023). Cooperative sensing of mitochondrial DNA by ZBP1 and cGAS promotes cardiotoxicity. Cell *186*, 3013–3032.e22. https://doi.org/10.1016/j.cell.2023.05.039.

46. Chen, R., Ishak, C.A., and De Carvalho, D.D. (2021). Endogenous Retroelements and the Viral Mimicry Response in Cancer Therapy and Cellular Homeostasis. Cancer Discov. *11*, 2707–2725. https://doi.org/10.1158/2159-8290.Cd-21-0506.

47. Koehler, H., Cotsmire, S., Zhang, T., Balachandran, S., Upton, J.W., Langland, J., Kalman, D., Jacobs, B.L., and Mocarski, E.S. (2021). Vaccinia virus E3 prevents sensing of Z-RNA to block ZBP1-dependent necroptosis. Cell Host Microbe *29*, 1266–1276.e5. https://doi.org/10.1016/j.chom.2021.05.009.

48. Glück, S., Guey, B., Gulen, M.F., Wolter, K., Kang, T.W., Schmacke, N.A., Bridgeman, A., Rehwinkel, J., Zender, L., and Ablasser, A. (2017). Innate immune sensing of cytosolic chromatin fragments through cGAS promotes senescence. Nat. Cell Biol. *19*, 1061–1070. https://doi.org/10.1038/ncb3586.

49. Liu, F., Wu, S., Ren, H., and Gu, J. (2011). Klotho suppresses RIG-I-mediated senescence-associated inflammation. Nat. Cell Biol. *13*, 254–262. https://doi.org/10.1038/ncb2167.

50. Gao, L., Bird, A.K., Meednu, N., Dauenhauer, K., Liesveld, J., Anolik, J., and Looney, R.J. (2017). Bone Marrow-Derived Mesenchymal Stem Cells From Patients With Systemic Lupus Erythematosus Have a Senescence-Associated Secretory Phenotype Mediated by a Mitochondrial Antiviral Signaling Protein-Interferon-β Feedback Loop. Arthritis Rheumatol. *69*, 1623–1635. https://doi.org/10.1002/art.40142.

51. He, H., Wang, Y., Zhang, X., Li, X., Liu, C., Yan, D., Deng, H., Sun, W., Yi, C., and Wang, J. (2024). Age-related noncanonical TRMT6-TRMT61A signaling impairs hematopoietic stem cells. Nat. Aging *4*, 213–230. https://doi.org/10.1038/s43587-023-00556-1.

52. Missiaen, R., Anderson, N.M., Kim, L.C., Nance, B., Burrows, M., Skuli, N., Carens, M., Riscal, R., Steensels, A., Li, F., and Simon, M.C. (2022). GCN2 inhibition sensitizes arginine-deprived hepatocellular carcinoma cells to senolytic treatment. Cell Metab. *34*, 1151–1167.e7. https://doi.org/10.1016/j.cmet.2022.06.010.

53. Pan, D., Bao, X., Hu, M., Jiao, M., Li, F., and Li, C.Y. (2022). SETDB1 Restrains Endogenous Retrovirus Expression and Antitumor Immunity during Radiotherapy. Cancer Res. *82*, 2748–2760. https://doi.org/10.1158/0008-5472.Can-21-3523.

54. Simon, M., Van Meter, M., Ablaeva, J., Ke, Z., Gonzalez, R.S., Taguchi, T., De Cecco, M., Leonova, K.I., Kogan, V., Helfand, S.L., et al. (2019). LINE1 Derepression in Aged Wild-Type and SIRT6-Deficient Mice Drives Inflammation. Cell Metab. *29*, 871–885.e5. https://doi.org/10.1016/j.cmet.2019.02.014.

55. De Cecco, M., Ito, T., Petrashen, A.P., Elias, A.E., Skvir, N.J., Criscione, S.W., Caligiana, A., Brocculi, G., Adney, E.M., Boeke, J.D., et al. (2019). L1 drives IFN in senescent cells and promotes age-associated inflammation. Nature *566*, 73–78. https://doi.org/10.1038/s41586-018-0784-9.

56. Lagnado, A., Leslie, J., Ruchaud-Sparagano, M.H., Victorelli, S., Hirsova, P., Ogrodnik, M., Collins, A.L., Vizioli, M.G., Habiballa, L., Saretzki, G., et al. (2021). Neutrophils induce paracrine telomere dysfunction and senescence in ROS-dependent manner. Embo j *40*, e106048. https://doi.org/10.15252/embj.2020106048.

57. Cai, Z., Jitkaew, S., Zhao, J., Chiang, H.C., Choksi, S., Liu, J., Ward, Y., Wu, L.G., and Liu, Z.G. (2014). Plasma membrane translocation of trimerized MLKL protein is required for TNF-induced necroptosis. Nat. Cell Biol. *16*, 55–65. https://doi.org/10.1038/ncb2883.

58. Weindel, C.G., Martinez, E.L., Zhao, X., Mabry, C.J., Bell, S.L., Vail, K.J., Coleman, A.K., VanPortfliet, J.J., Zhao, B., Wagner, A.R., et al. (2022). Mitochondrial ROS promotes susceptibility to infection via gasdermin D-mediated necroptosis. Cell *185*, 3214–3231.e23. https://doi.org/10.1016/j.cell.2022.06.038.

59. Yue, Z., Nie, L., Ji, N., Sun, Y., Zhu, K., Zou, H., Song, X., Chen, J., and Wang, Q. (2023). Hyperglycaemia aggravates periodontal inflamm-aging by promoting SETDB1-mediated LINE-1 de-repression in macrophages. J. Clin. Periodontol. *50*, 1685–1696. https://doi.org/10.1111/jcpe.13871.

60. Matsumura, Y., Nakaki, R., Inagaki, T., Yoshida, A., Kano, Y., Kimura, H., Tanaka, T., Tsutsumi, S., Nakao, M., Doi, T., et al. (2015). H3K4/H3K9me3 Bivalent Chromatin Domains Targeted by Lineage-Specific DNA Methylation Pauses Adipocyte Differentiation. Mol. Cell *60*, 584–596. https://doi.org/10.1016/j.molcel.2015.10.025.

61. Rodriguez, D.A., Quarato, G., Liedmann, S., Tummers, B., Zhang, T., Guy, C., Crawford, J.C., Palacios, G., Pelletier, S., Kalkavan, H., et al. (2022). Caspase-8 and FADD prevent spontaneous ZBP1 expression and necroptosis. Proc. Natl. Acad. Sci. USA *119*, e2207240119. https://doi.org/10.1073/pnas.2207240119.

62. Shih, C., Padhy, L.C., Murray, M., and Weinberg, R.A. (1981). Transforming genes of carcinomas and neuroblastomas introduced into mouse fibroblasts. Nature *290*, 261–264. https://doi.org/10.1038/290261a0.

63. Hsu, C.C., Wang, C.Y., Manne, R.K., Cai, Z., Penugurti, V., Kant, R., Bai, L., Pan, B.S., Chen, T., Chen, Y.R., et al. (2025). ALDH4A1 functions as an active component of the MPC complex maintaining mitochondrial pyruvate import for TCA cycle entry and tumour suppression. Nat. Cell Biol. *27*, 847–862. https://doi.org/10.1038/s41556-025-01651-8.

64. Bender, F.C., Reymond, M.A., Bron, C., and Quest, A.F. (2000). Caveolin-1 levels are down-regulated in human colon tumors, and ectopic expression of caveolin-1 in colon carcinoma cell lines reduces cell tumorigenicity. Cancer Res. *60*, 5870–5878.

65. Wu, L., Hong, X., Yang, C., Yang, Y., Li, W., Lu, L., Cai, M., Cao, D., Zhuang, G., and Deng, L. (2023). Noncanonical MAVS signaling restrains dendritic cell-driven antitumor immunity by inhibiting IL-12. Sci. Immunol. *8*, eadf4919. https://doi.org/10.1126/sciimmunol.adf4919.

STAR★METHODS

KEY RESOURCES TABLE

REAGENT or RESOURCE	SOURCE	IDENTIFIER
Antibodies		
Anti-mouse FcR (CD16/CD32)	Bio X Cell	Cat#BE0307; RRID: AB_2736987
Anti-mouse-CD45.2-BV785	BioLegend	Cat#109839; RRID: AB_2562604
Anti-mouse-CD8-Alexa Fluor 700	BioLegend	Cat#100730; RRID: AB_493703
Anti-mouse-CD8-BV650	BioLegend	Cat#100742; RRID: AB_2563056
Anti-mouse-TCRβ-FITC	eBioscience	Cat#11-5961-82; RRID: AB_2574644
Anti-mouse-Ki-67-BV605	BioLegend	Cat#652413; RRID: AB_2562664
Anti-mouse-CD45.1-FITC	ebioscience	Cat#11-0453-82; RRID: AB_465058
Anti-mouse-IFN-γ-PE	BioLegend	Cat#505808; RRID: AB_315402
Anti-mouse-TNF-α-BV421	BD Biosciences	Cat#48-7321-82; RRID: AB_2198703
Anti-mouse-Ly6C-BV605	BioLegend	Cat#128036; RRID: AB_2562352
Anti-mouse-Ly6G-BV711	BioLegend	Cat#127608; RRID: AB_1186104
Anti-mouse-F4/80-BV421	BioLegend	Cat#123132; RRID: AB_2563102
Anti-mouse-CD11c-APC	BioLegend	Cat#117310; RRID: AB_313778
Anti-mouse-CD11b-PE-Cy7	BioLegend	Cat#101216; RRID: AB_312798
Anti-mouse-MHC II-PerCP/Cy5.5	BioLegend	Cat#107626; RRID: AB_2191072
Anti-mouse-CD4-BV510	BioLegend	Cat#116025; RRID: AB_ 2800580
Anti-mouse-NK1.1-APC-Cy7	BioLegend	Cat#108724; RRID: AB_830870
Anti-mouse-CD80 PE	BioLegend	Cat#104707; RRID: AB_313128
Annexin V-FITC	BD Pharmingen	Cat#556419; RRID: AB_2665412
Fixable Viability Stain 780	BD Biosciences	Cat#565388; RRID: AB_2869673
Fixable Viability Stain 700	BD Biosciences	Cat#564997; RRID: AB_2869637
*InVivo*MAb anti-human/rat HER2 (neu)	Bioxcell	Cat#BE0277; RRID: AB_2687800
*InVivo*MAb anti-mouse CD8a	BioXCell	Cat#BE0061; RRID: AB_1125541
*InVivo*Plus anti-mouse CD4	BioXCell	Cat#BP0003-1; RRID: AB_1107636
*InVivo*Plus anti-mouse IFNAR1	BioXCell	Cat#BP0241; RRID: AB_2687723
Anti-Z-DNA/Z-RNA (Z22)	Absolute antibody	Cat#Ab00783–3.0; RRID: AB_2820286
Mouse monoclonal anti-dsRNA	SCICONS	Cat#10010200; RRID: AB_2651015
Rabbit Polyclonal anti-Tubulin	Proteintech	Cat#4970; RRID: AB_2223172
Phospho-STING(Ser366) (E9A9K) Rabbit mAb	Cell Signaling Technology	Cat#50907; RRID: AB_2827656
STING(D2P2F) Rabbit mAb	Cell Signaling Technology	Cat#13647; RRID: AB_2732796
Mouse monoclonal anti-ZBP1	AdipoGen Life Sciences	Cat#AG-20B-0010; RRID: AB_2490191
Rat monoclonal anti-MLKL	Millipore	Cat#MABC604; RRID: AB_2820284
Phospho-MLKL (Ser345) (D6E3G) Rabbit mAb	Cell Signaling Technology	Cat#37333; RRID: AB_2799112
Stat1 (D1K9Y) Rabbit mAb	Cell Signaling Technology	Cat#14994; RRID: AB_2737027
Phospho-Stat1 (Tyr701) (58D6) Rabbit mAb	Cell Signaling Technology	Cat#9167; RRID: AB_561284
Lamin B1 (D9V6H) Rabbit mAb	Cell Signaling Technology	Cat#13435; RRID: AB_2737428
SETDB1 Polyclonal antibody	Proteintech	Cat#11231-1-AP; RRID: AB_2186069
RIP3 (D4G2A) Rabbit mAb	Cell Signaling Technology	Cat#95702; RRID: AB_2721823
MAVS Antibody	Cell Signaling Technology	Cat# 4983; RRID: AB_823566
Rabbit monoclonal anti-Flag (DYKDDDDK)	Cell Signaling Technology	Cat#14793; RRID: AB_2572291
Bacterial and virus strains		
DH5α competent cells	Tiangen Biotech	Cat#CB101

(*Continued on next page*)

Continued

REAGENT or RESOURCE	SOURCE	IDENTIFIER
Chemicals, peptides, and recombinant proteins		
Collagenase Type I	Worthington Biochemical	Cat#LS004186
Lipofectamine 3000	Invitrogen	Cat# L3000015
DNase I	Sigma	Cat#DN25; CAS: 9003-98-9
RNase III	NEB	Cat#M0245S
DNA transfection reagent	Neofect Biotech	Cat#TF201201
GMPO Polybrene	Genomeditech	Cat#GM-040901B
TRIzol Reagent	Invitrogen	Cat#15596018
Fixation/Perm Diluent	eBioscience	Cat#00-5223-56
Fixation/Permeabilization Concentrate	eBioscience	Cat#00-5123-43
Permeabilization buffer 10×	eBioscience	Cat#00-8333-56
Cell stimulation cocktail plus protein transport inhibitor (500×)	eBioscience	Cat#00-4975-93
SYTOX Orange Nucleic Acid Stain	Invitrogen	Cat#S11368
Protein transport inhibitor	eBioscience	Cat#00-4980-93
Trypan Blue	Gibco	Cat#15250061
Puromycin Dihydrochloride	Beyotime Biotechnology	Cat#ST551
Recombinant murine IFN-γ	PeproTech	Cat#315-05
Recombinant murine IL-15	PeproTech	Cat#210-15
Recombinant murine IL-7	PeproTech	Cat#217-17
5AZA-2′-deoxycytidine	Sigma-Aldrich	Cat#A3656
Fludarabine	Med Chem Express	Cat#HY-B0069
Navitoclax	Selleck	Cat#S1001
H-151	Tocris Bioscience	Cat#6675
Critical commercial assays		
EasySep™ Mouse CD8a Positive Selection Kit II	STEMCELL Technologies	Cat#19853
Senescence β-Galactosidase Cell Staining Kit	Cell Signaling Technology	Cat#9860
SPiDER-βGal	DOJINDO	Cat#SG02
MS IFN-GMA BD ELISPOT SET	BD Biosciences	Cat#551083
E.Z.N.A.® Endo-Free Plasmid Midi Kit	Omega Bio-tek	Cat#D6904
BCA Protein Assay Kit	Novoprotein	Cat#PA002
Hifair® AdvanceFast 1st Strand cDNA Synthesis SuperMix for qPCR	Yeasen Biotechnology	Cat#11155ES60
Subcellular structure nuclear and cytoplasmic protein extraction kit	BOSTER	Cat#AR0106
DNA ligation kit-Ligation High	TOYOBO	Cat#LGK-100
Experimental models: Cell lines		
MC38	Lab of Yang-Xin Fu	N/A
MC38-OVA	Lab of Ralph R. Weichselbaum	N/A
MC38-ZBP1$^{-/-}$	This paper	N/A
MC38-OVA-ZBP1$^{-/-}$	This paper	N/A
MC38-MLKL$^{-/-}$	This paper	N/A
MC38-SETDB1$^{-/-}$	This paper	N/A
MC38-MAVS$^{-/-}$	This paper	N/A
MC38-SETDB1&ZBP1$^{-/-}$	This paper	N/A
MC38-SETDB1&MLKL$^{-/-}$	This paper	N/A
MC38-SETDB1-OE	This paper	N/A
TUBO	Cell bank of the Chinese academy of sciences	N/A

(*Continued on next page*)

Continued

REAGENT or RESOURCE	SOURCE	IDENTIFIER
TUBO-ZBP1$^{-/-}$	This paper	N/A
TUBO-MLKL$^{-/-}$	This paper	N/A
TUBO-SETDB1$^{-/-}$	This paper	N/A
3T3	Lab of Xuanming Yang	N/A
3T3-ZBP1$^{-/-}$	This paper	N/A
3T3-ZBP1$^{-/-}$- pBOBI	This paper	N/A
3T3-ZBP1$^{-/-}$-Flag-ZBP1	This paper	N/A
3T3-ZBP1$^{-/-}$-Flag-ΔZα2	This paper	N/A
3T3-ZBP1$^{-/-}$-Flag-ΔRHIMA	This paper	N/A
3T3-ZBP1$^{-/-}$-Flag-ΔRHIMB	This paper	N/A
3T3-ZBP1$^{-/-}$-Flag-ΔC	This paper	N/A
HEK293T	Cell bank of the Chinese academy of sciences	N/A
Experimental models: Organisms/strains		
C57BL/6 mice	Shanghai Slaccas	N/A
BALB/c mice	Shanghai Slaccas	N/A
OT-I mice	Lab of Fubin Li	N/A
Oligonucleotides		
All oligo sequences used in this paper are listed in Table S1.	This Paper	N/A
Recombinant DNA		
PsPAX2	Lab of Xin-Yuan Liu	N/A
pMD2.G	Lab of Xin-Yuan Liu	N/A
SETDB1	Youze Biotechnology	N/A
Vector	Youze Biotechnology	N/A
pBOBI	Lab of Ben Lu	N/A
Flag-ZBP1	Lab of Ben Lu	N/A
Flag-ΔZα2	Lab of Ben Lu	N/A
Flag-ΔRHIMA	Lab of Ben Lu	N/A
Flag-ΔRHIMB	Lab of Ben Lu	N/A
Flag-ΔC	Lab of Ben Lu	N/A
Software and algorithms		
Prism graphpad	GraphPad Prism software	Version 8.0
FlowJo	Tree Star software	Version 10.0
Photoshop	Adobe Systems	Version CS6
ImageJ	Java	Version 1.8.0

EXPERIMENTAL MODEL AND STUDY PARTICIPANT DETAILS

Mice

Female C57BL/6J (WT) and BALB/c (WT) mice aged 6-8-week-old were purchased from Shanghai SLAC Animal Center (Shanghai, China). OT-I mice were kind gifts from Prof. Fubin Li at Shanghai Institute of Immunology (Shanghai, China). All the mice were placed under specific pathogen–free conditions and the animal studies were approved by the Institutional Animal Care and Use Committee of Shanghai Jiao Tong University.

Cells and cell culture

MC38, MC38-OVA, TUBO, 3T3 cell lines were cultured at 37°C with 5% CO_2 in Dulbecco Modified Eagle Media (DMEM) with 100 U/mL penicillin, 10 mM HEPES and 100 μg/mL streptomycin and 10% fetal bovine serum (Excell Bio). Phosphate-buffered saline (PBS) was purchased from TBD Science Biotech. All the cells were tested negative for mycoplasma contamination. ZBP1$^{-/-}$ MC38, MLKL$^{-/-}$ MC38, SETDB1$^{-/-}$ MC38, MAVS$^{-/-}$ MC38, SETDB1&ZBP1 DKO MC38, SETDB1&MLKL DKO MC38, ZBP1$^{-/-}$ TUBO, MLKL$^{-/-}$ TUBO, SETDB1$^{-/-}$ TUBO, ZBP1$^{-/-}$MC38-OVA and ZBP1$^{-/-}$3T3 cell lines were generated using CRISPR-Cas9 (as described below).

METHOD DETAILS

Plasmids construction and transfection

Plasmids encoding ZBP1 truncated mutations were kind gifts from Prof. Ben Lu at the Central South University.[23] All constructs were cloned into pBOBI lentiviral vectors with no tag or FLAG tag. The lenti-SETDB1 and empty vector were purchased from Youze Biotechnology (Changsha, China). 293T cells were co-transduced with lentiviral packaging plasmids (psPax2/pMD2.G) and target plasmids, and the supernatants of culture medium were collected 48h later for transfection with 10μg/mL polybrene in ZBP1$^{-/-}$3T3 cells or MC38 cells.

ZBP1$^{-/-}$ MC38, MLKL$^{-/-}$ MC38, SETDB1$^{-/-}$ MC38, MAVS$^{-/-}$ MC38, SETDB1&ZBP1 DKO MC38, SETDB1&MLKL DKO MC38, ZBP1$^{-/-}$ TUBO, MLKL$^{-/-}$ TUBO, SETDB1$^{-/-}$ TUBO, ZBP1$^{-/-}$MC38-OVA and ZBP1$^{-/-}$3T3 cell lines were conducted using CRISPR-Cas9 plasmid crispr-V2. The annealed sgRNA oligos were introduced into plasmid crispr-V2 as previously and transduced with Lipofectamine 3000 (Invitrogen) as manufacturers' instructions (See Table S1).[12] To generate stable cell lines, 2μg/mL puromycin was used to selected transfected cells and the related-gene knockdown was verified by western blotting.

Pharmacological treatment

The DNMT inhibitor, 5-aza-2′-deoxycytidine (5AZA; Sigma-Aldrich), was reconstituted in DMSO as 60 mM stocks and kept at −80°C. For *in vitro* 5AZA treatment, cells were seeded at the density of 1×10^5 overnight, followed by 5AZA (0.3μM), or vehicle treatment for one day. The next day, cells were cultured with drug-free medium and kept in culture for another 4 days. Cells were then used for the downstream assays. For combined therapy, 5AZA (0.3μM) was treated once at day 1 while anti-IFNAR blockage antibody (200μg/mL; Bioxcell), Fludarabine (20μM; Med Chem Express) were sustained for 5 days.

For combined treatment of 5AZA (0.15μM) and anti-HER2 antibody (anti-HER2 mAb, 1.5μg/mL; Bioxcell) *in vitro*, TUBO cells were seeded before night. Cells were treated with 5AZA at day 1, and anti-HER2 mAb was continued to sustained for 5 days. To displaying the time course changes of combined therapy, cell samples were collected on day 0, 2 and 5, respectively. For combined therapy, 5AZA was treated at day 1 while anti-HER2 antibody, an STING inhibitor H-151 (5μm; Tocris Bioscience) or Fludarabine were sustained for 5 days. For elimination of senescent cells, 0.25μM ABT-263 (Navitoclax; Selleck) was maintained for 5 days with daily refreshment. Cells were collected for later experiments.

In vivo tumor models

To explore the therapeutic effects of 5AZA on tumor growth, C57 mice were subcutaneously inoculated with 5×10^5 CRISPR-Ctrl-MC38, ZBP1$^{-/-}$ MC38, MLKL$^{-/-}$ MC38 or SETDB1&ZBP1$^{-/-}$ MC38 cells, which were resuspended in PBS. Before mean tumor volume reached 100mm^3 (day 9), intratumoral treatment (i.t.) was initiated with 2mg/kg 5AZA once a week for 2 weeks. In MC38-OVA model, lymph node cells of OT-I mice were stimulated with 250 ng/mL OVA peptide for 1 day and cultured with mIL-7 (10ng/mL) and mIL-15 (10ng/mL) for another 4–5 days. C57 mice were subcutaneously inoculated with 2×10^6 CRISPR-Ctrl or ZBP1$^{-/-}$ MC38-OVA tumor cells. Activated OT-I CD8$^+$ T cells (2×10^6) were intravenously transferred and 2mg/kg 5AZA were intratumoral initiated in these tumor-bearing mice on day 8. Mice in the CRISPR-Ctrl group were given the same volume of PBS.

To see the effects of the combined therapy of anti-HER2 mAb and 5AZA on tumor growth, BALB/c mice were subcutaneously inoculated with 5×10^5 CRISPR-Ctrl, ZBP1$^{-/-}$ TUBO or MLKL$^{-/-}$ TUBO cells resuspending in PBS. Before mean tumor volume reached 100mm^3, treatments were initiated with 2mg/kg 5AZA (once a week for 2 weeks, i.t.), 50μg anti-HER2 antibody (at day 9, intraperitoneally, i.p.), or 2mg/kg 5AZA combined with 50μg anti-HER2 antibody. Tumors volumes were measured twice a week subsequently. Mice in the CRISPR-Ctrl groups were given the same volume of PBS. To explore whether adaptive immunity was required for combined therapy-mediated tumor regression, TUBO bearing mice were intraperitoneally given anti-CD8-depleting antibody (250μg/mouse; Bio X Cell) or anti-CD4-depleting antibody (250μg/mouse; Bio X Cell) in conjunction with combined therapy. For elimination of CD8$^+$ or CD4$^+$ T cells, depleting antibodies were administered on a repeating regimen of every 4 days since day 7.[65] For confirmation of depletions for CD8$^+$ T cells and CD4$^+$ T cells, immune cells in circulating blood were collected for flow cytometry analysis on day 12.

Flow cytometry

To obtain the single-cell suspension, subcutaneous tumors were collected on 7 days after first drug administration, cut into small pieces, and digested with 1 mg/mL collagenase I and 0.2 mg/mL deoxyribonuclease I for half an hour. For cell surface marker staining, cells suspension was incubated with anti-FcR at 4°C for 15 min, and at 4°C for 30 min with antibody cocktail of anti-CD8, anti-TCRβ, anti-CD45.2, anti-CD45.1, anti-Ly6C, anti-Ly6G, anti-F4/80, anti-CD11b, anti-CD11c, anti-MHC class II, anti-CD4, anti-NK1.1, anti-CD80 antibodies and Live/Dead. For intracellular staining, cells were fixed with Fixation/Permeabilization Buffer (Invitrogen) at 4°C for 1 h, and stained for 40 min at 4°C with corresponding antibody cocktails. To see T cell function in TME, collected cells were co-cultured with Cell Stimulation Cocktail (plus protein transport inhibitors) (eBioscience) for 4 h followed by flow cytometry staining. Percentages of IFN$^+$, TNF$^+$ and Ki-67$^+$ of CD8$^+$ T cells in TME were evaluated with LSR ×20.

For cell death analysis, treated cells were assessed by SYTOX Orange Nucleic Acid Stain (Invitrogen) and Annexin V (BD Pharmingen) staining. The percentages of double-positive cells were analyzed.

ELISPOT assay

For tumor-specific $CD8^+$ T cell analysis, draining lymph nodes (DLN) or spleens were obtained 7 days after first treatment and $CD8^+$ T cells were positively selected by EasySep Mouse CD8a Positive Selection Kit II (STEMCELL). Pre-exposed to murine IFN-γ (20 ng/mL) for one day, MC38 cells were co-cultured with purified $CD8^+$ T cells (2×10^5) at a ratio of 1:10 for 48 h. ELISPOT assays were introduced to calculate IFN-γ spots as manufacturing procedure (BD Biosciences).

Prediction of transcription factor of ZBP1

The Jasper database (https://jaspar.genereg.net/) and the Animal TFBD database (http://bioinfo.life.hust.edu.cn/) were both used to predict the specific binding site between downstream transcription factor of type I interferon pathway and ZBP1. Through the interaction of the two databases, the downstream specific transcription factor of ZBP1 and the binding sites in ZBP1 promoter regions were predicted.

Prognostic analysis of ZBP1 in $HER2^+$ BRCA

The GEPIA database (http://gepia2.cancer-pku.cn/#index) was employed to analyze the correlation between ZBP1 expression and overall survival among $HER2^+$ BRCA in 15 years. A statistically significance was suggested as mentioned.

Western blot and co-immunoprecipitation assay

For protein extraction, pretreated cells were lysed directly in cell lysis buffer and quantified using a BCA protein assay kit (Novoprotein). For nuclear protein extraction, pretreated cells were collected and conducted as manufacturer's instructions (BOSTER). Fifty micrograms protein were loaded on SurePAGE gels, electrophoresed, blotted to polyvinylidene difluoride (PVDF) membranes (GenScript). The PVDF membranes were blocked with 5% BSA (Neobioscience) and incubated with the primary and corresponding secondary antibodies. The target bands were than developed with the ECL kit (Biodragon). The primary antibodies were obtained as following: anti-ZBP1 (1:1000; AdipoGen), anti-MLKL (1:1000; Millipore), anti–phospho-MLKL (1:1000; CST), anti–STAT1(1:1000; CST), anti–phospho-STAT1 (1:1000; CST), anti–Lamin B (1:1000; CST), anti-SETDB1 (1:1000; Proteintech), anti–Flag (1:1000; CST), anti-RIPK3 (1:1000; CST), anti-MAVS (1:1000; CST), anti-Tubulin (1:3000; Proteintech).

To detect ZBP1 binding proteins, ZBP1 gene was cloned into a lentiviral pBOB-Flag vector. $ZBP1^{-/-}$3T3 cells were transfected with the lentiviruses for 2 days. Treated cells were collected and lysed in immunoprecipitation (IP) buffer with protease inhibitors (New Cell & Molecular Biotech). The supernatants were rotated overnight with 2 μg of corresponding primary antibodies at 4°C, then mixed with Protein A/G agarose for 2h. Immunoprecipitants were washed four times, eluted, and heated at 95°C for 10 min with sample buffer. Immunoprecipitants were detected using western-blot analysis.

RNA purification and RT-PCR

TUBO cells were stimulated with 5AZA, anti-HER2 mAb, or 5AZA in conjunction with anti-HER2 mAb with above methods. Total RNA of TUBO cells was extracted with TRIzol reagent (Invitrogen), and cDNA was synthesized with reverse transcription kit (Yeasen Biotechnology). Real-time PCR was conducted by ABI 7500 PCR system. All the primer sequences were listed and obtained data were normalized to *Gapdh* (Table S1).

Immunofluorescence imaging

To assess Z-RNA in 5AZA-activated MC38 or anti-HER2 mAb and 5AZA-induced TUBO, cells were fixed with 4% PFA (Servicebio), permeabilized with 0.5% Triton X-100, and incubated with mouse anti-Z-NA (Z22 clone Ab, 1:200, Absolute antibody) or mouse anti-dsRNA (J2 clone, 1:50, Scicons) primary antibody overnight at 4°C, respectively. After incubated for 1 h at room temperature with Goat anti-Mouse IgG (1:2000; Thermo Fisher Scientific), fixed cells were subjected to DAPI (5μg/mL, ABclonal) staining for 15 min. In some cases, proteinase K (Bioss) treatment was performed with (0.008 U/mL) for 30 min at 37°C post-fixation. RNaseIII (40 IU/mL; NEB) was also used at 37°C for 1h. The fluorescent signals were determined by laser confocal microscopy.

In situ proximity ligation assay (PLA)

3T3 cell lines are well-suited for gene editing studies and widely used in tumorigenesis research, which may indicate that cancer cells share similar molecular mechanism. To determine the interaction between Z-RNA and Flag-tagged ZBP1 mutants, $ZBP1^{-/-}$ 3T3 cells with Flag-tagged ZBP1 mutants were generated. ZBP1-deficient 3T3 cells with Flag-tagged ZBP1 mutants were fixed and permeabilized with 0.5% Triton X-100 for 20 min. Fixed cells were incubated with pair of different species primary antibodies targeting Z-RNA (mouse monoclonal) or Flag (rabbit monoclonal) at 4°C overnight. *In situ* PLA was performed as manufacturer's instructions (Sigma-Aldrich).

Senescence-associated β1 galactosidase (SA-β-gal)

Staining was conducted as the manufacturer's instructions (Cell Signaling technology). Briefly, treated tumor cells were fixed with provided fixative solution and stained with β-gal staining solution in incubator without CO_2 overnight. The percentages of SA-β-gal positive cells in total cells were calculated with ImageJ.

The co-staining of Z-RNA and β-gal was performed using the Cellular Senescence Detection Kit-SPiDER-βGal (DOJINDO). Briefly, treated cells were washed with PBS, fixed in 4% PFA for 3 min, and incubated with SPiDER-βGal in the dark for 30min at 37°C without CO_2. Washed with PBS, cells were subjected to immunofluorescence staining of Z-RNA as the normal procedure.[34]

Cell isolation by flow cytometry

To isolate senescent cells ($SPiDER^+$) from non-senescent cells ($SPiDER^-$), SPiDER-βgal staining was used. Staining was conducted as the manufacturer's instructions and treated cells were sorted using the FACS Aria II (BD) system.

Cell growth rate assay

To evaluate the impact of ZBP1 knockout on cell proliferation, we compared the cell numbers of CRISPR-Ctrl and ZBP1 KO in MC38 and TUBO cell lines over a 5-day period. Cells were seed in twelve-well plates at the density of 5×10^4 per well and cultured at 37°C with 5% CO_2 in DMEM. Measurements of cell numbers were taken at multiple time points over a 5-day period, specifically at 0, 1, 2, 3, 4, and 5 days post-seeding, allowing for the assessment of the effects of ZBP1 knockout on MC38 and TUBO cell growth.

QUANTIFICATION AND STATISTICAL ANALYSIS

Statistical analyses were performed with GraphPad Prism 8.0 software. For comparison among tumor growth, two-way analysis of variance (ANOVA) with Sidak's multiple comparisons test was used. For comparisons between two groups, a two-tailed unpaired Student's t-test was applied when data displayed a normal distribution, whereas a two-tailed unpaired Student's t-test with Welch's correction was used when variances showed different. For comparing parameter among multiple groups, one-way ANOVA with Dunnett's multiple comparison tests was applied. Data are presented as mean ± SEM. Significance is indicated as follows: $*p < 0.05$; $**p < 0.01$; $***p < 0.001$; $****p < 0.0001$; ns, no significant difference.

Cell Reports, Volume *44*

Supplemental information

ZBP1 pathway promotes tumor immunogenicity in the combination of anti-HER2 therapy and epigenetic therapy

Qishan Wang, Zhihao Wu, Yuanqin Yang, Chao Yang, Haoran Deng, Xingyue Zhou, Shuting Xu, Lingling Wu, Xiaochuan Hong, Xueni Yu, Lu Lu, and Liufu Deng

Supplemental Information

Supplemental Figures and Figure Legends

Supplementary Figure 1

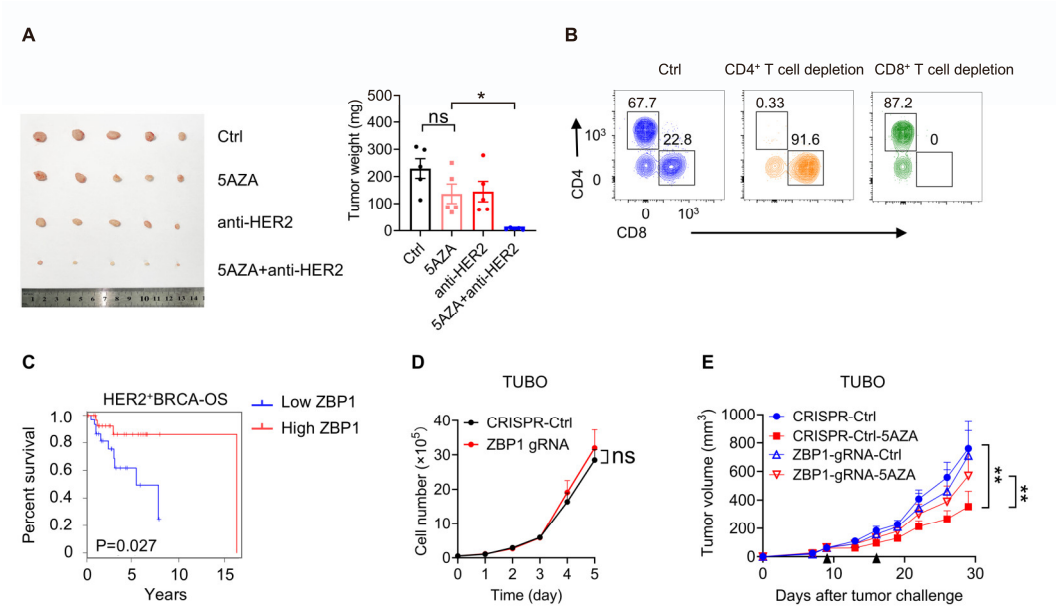

Figure S1. Combination therapy of anti-HER2 mAb and 5AZA generated better tumor control in HER2⁺ BRCA. Related to Figure 1. (A) Quantification of TUBO tumor weights on day 16 (n=5). (B) Confirmation of depletions for CD8⁺ T cells and CD4⁺ T cells from circulating blood on day 12 (n=4). BALB/c mice were subcutaneously inoculated with 5 × 10^5 TUBO cells. TUBO bearing mice were intraperitoneally given 250μg anti-CD8-depleting antibody or anti-CD4-depleting antibody on a repeating regimen of every 4 days since day 7. Mice in the Ctrl group were given the same volume of PBS intraperitoneally. Flow cytometry analysis of the immune cells in circulating blood was conducted on day 12. (C) ZBP1-dependent overall survival among HER2⁺ BRCA tumors from GEPIA. (D) Cell growth rate of CRISPR-Ctrl and ZBP1$^{-/-}$ TUBO cells at 0, 1, 2, 3, 4, and 5 days post-seeding. (E) 5AZA-mediated therapeutic effects depended on ZBP1 presence in TUBO tumors. The black arrows indicated 5AZA monotherapy (n=5). Data are represented as means ± SEM. *P< 0.05 and ** P < 0.01 by one-way ANOVA in (A) and two-way ANOVA in (D and E).

Supplementary Figure 2

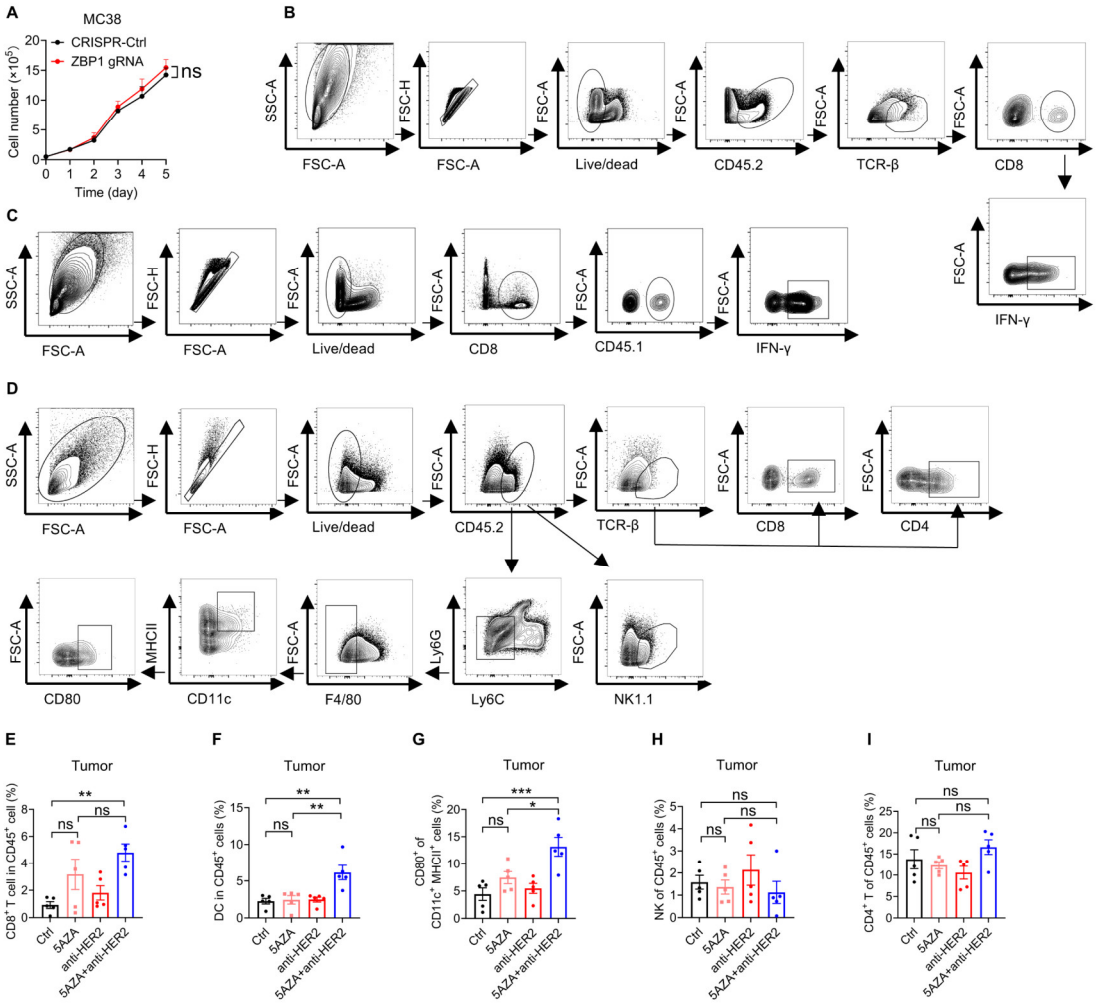

Figure S2. Cell growth rate and gating strategy of intra-tumoral immune cells. Related to Figure 2. (A) Cell growth rate of CRISPR-Ctrl and ZBP1$^{-/-}$ MC38 cells at 0, 1, 2, 3, 4, and 5 days post-seeding. (B) Gating strategy of CD8$^+$ T cell (CD45.2$^+$TCR-β$^+$CD8$^+$) function markers from CRISPR-Ctrl and ZBP1$^{-/-}$ MC38 tumors after indicated treatments. (C) Gating strategy of adoptively transferred OT-I CD8$^+$ T cell (CD8$^+$CD45.1$^+$) function markers from MC38-OVA tumors after indicated treatments. (D) Gating strategy of intra-tumoral CD8$^+$ T cells, DC, NK cells, CD4$^+$ T cells from TUBO tumors by flow cytometry. (E) Quantitative analysis of CD8$^+$ T cell (CD45.2$^+$TCR-β$^+$CD8$^+$) percentage on day 16 post inoculation with TUBO cells after indicated treatments (n = 5). (F) Quantitative analysis of DC (CD45.2$^+$Ly6G$^-$Ly6C$^-$F4/80$^-$ CD11c$^+$MHC II$^+$) percentage on day 16 post inoculation with TUBO cells after indicated treatments (n = 5). (G) Quantification of CD80 expression on DC on day 16 post inoculation with TUBO cells after indicated treatments (n = 5). (H) Quantitative analysis of NK cell (CD45.2$^+$NK1.1$^+$) percentage on day 16 post inoculation with TUBO cells after indicated treatments (n = 5). (I) Quantitative analysis of CD4$^+$ T cell (CD45.2$^+$TCR-β$^+$CD4$^+$) percentage on day 16 post inoculation with TUBO cells after indicated treatments (n = 5). Data are represented as means ± SEM. *P< 0.05 ** P < 0.01 and *** P < 0.001 by two-way ANOVA in (A) and one-way ANOVA in (E-I).

Supplementary Figure 3

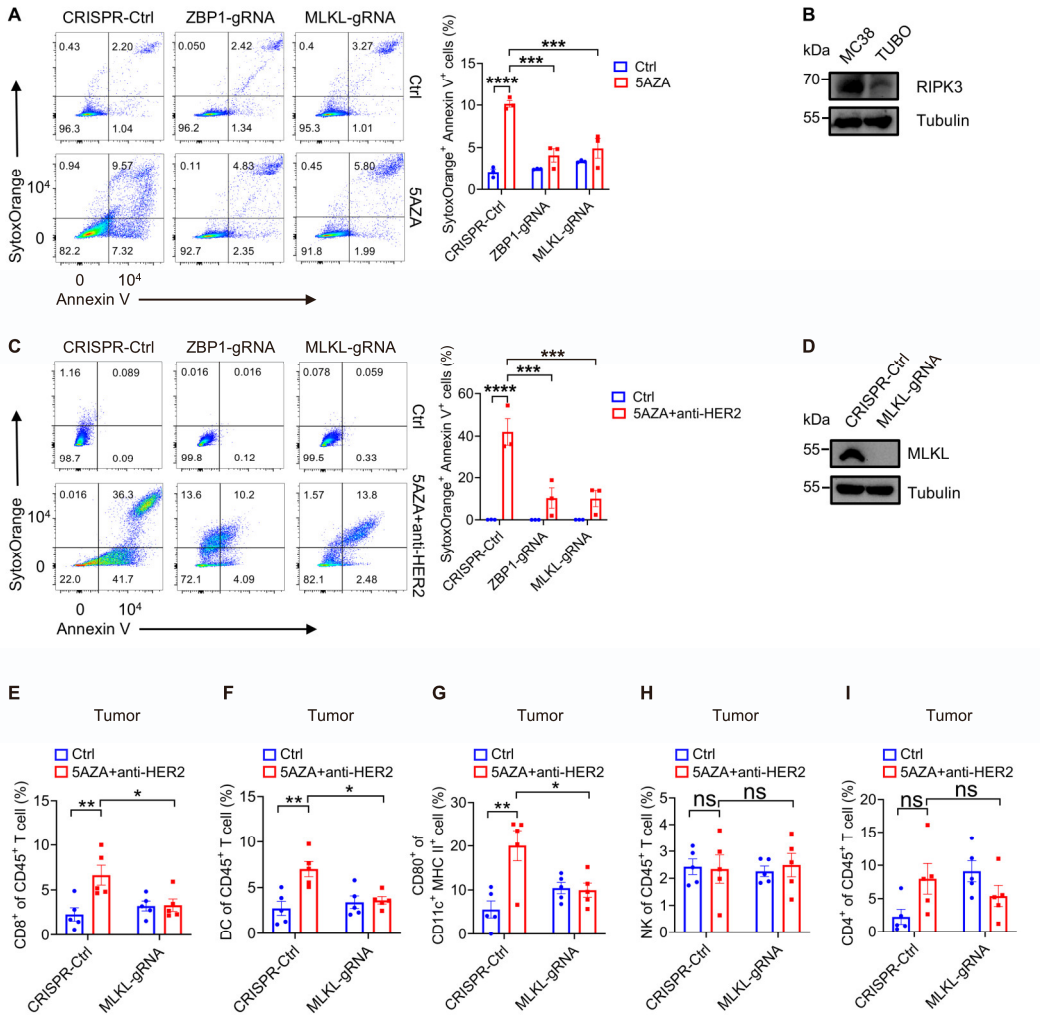

Figure S3. ZBP1-MLKL pathway mediates tumor cell death under 5AZA treatment and combined therapy. Related to Figure 3. (A) Percentage of SytoxOrange$^+$ Annexin V$^+$ cells in ZBP1 and MLKL KO MC38 cells after 5AZA treatment on day 5. (B) Expression levels of RIPK3 in MC38 and TUBO cells on day 5. (C) Percentage of SytoxOrange$^+$ Annexin V$^+$ cells in ZBP1 and MLKL KO TUBO cells after synergized treatment on day 5. (D) MLKL expression in CRISPR-Ctrl and MLKL$^{-/-}$ TUBO cells on day 5 post-seeding. (E) Quantitative analysis of CD8$^+$ T cell (CD45.2$^+$TCR-β$^+$CD8$^+$) percentage on day 16 post inoculation with CRISPR-Ctrl, MLKL$^{-/-}$ TUBO cells after indicated treatments (n = 5). (F) Quantitative analysis of DC (CD45.2$^+$Ly6G$^-$ Ly6C$^-$F4/80$^-$CD11c$^+$MHC II$^+$) percentage on day 16 post inoculation with CRISPR-Ctrl, MLKL$^{-/-}$ TUBO cells after indicated treatments (n = 5). (G) Quantification of CD80 expression on DC on day 16 post inoculation with CRISPR-Ctrl, MLKL$^{-/-}$ TUBO cells after indicated treatments (n = 5). (H) Quantitative analysis of NK cell (CD45.2$^+$NK1.1$^+$) percentage on day 16 post inoculation with CRISPR-Ctrl, MLKL$^{-/-}$ TUBO cells after indicated treatments (n = 5). (I) Quantitative analysis of CD4$^+$ T cell (CD45.2$^+$TCR-β$^+$CD4$^+$) percentage on day 16 post inoculation with CRISPR-Ctrl, MLKL$^{-/-}$ TUBO cells after indicated treatments (n = 5). Data are represented as means ± SEM. * P < 0.05, ** P < 0.01, *** P < 0.001 and **** P < 0.0001 by one-way ANOVA in (A, C and E-I).

Supplementary Figure 4

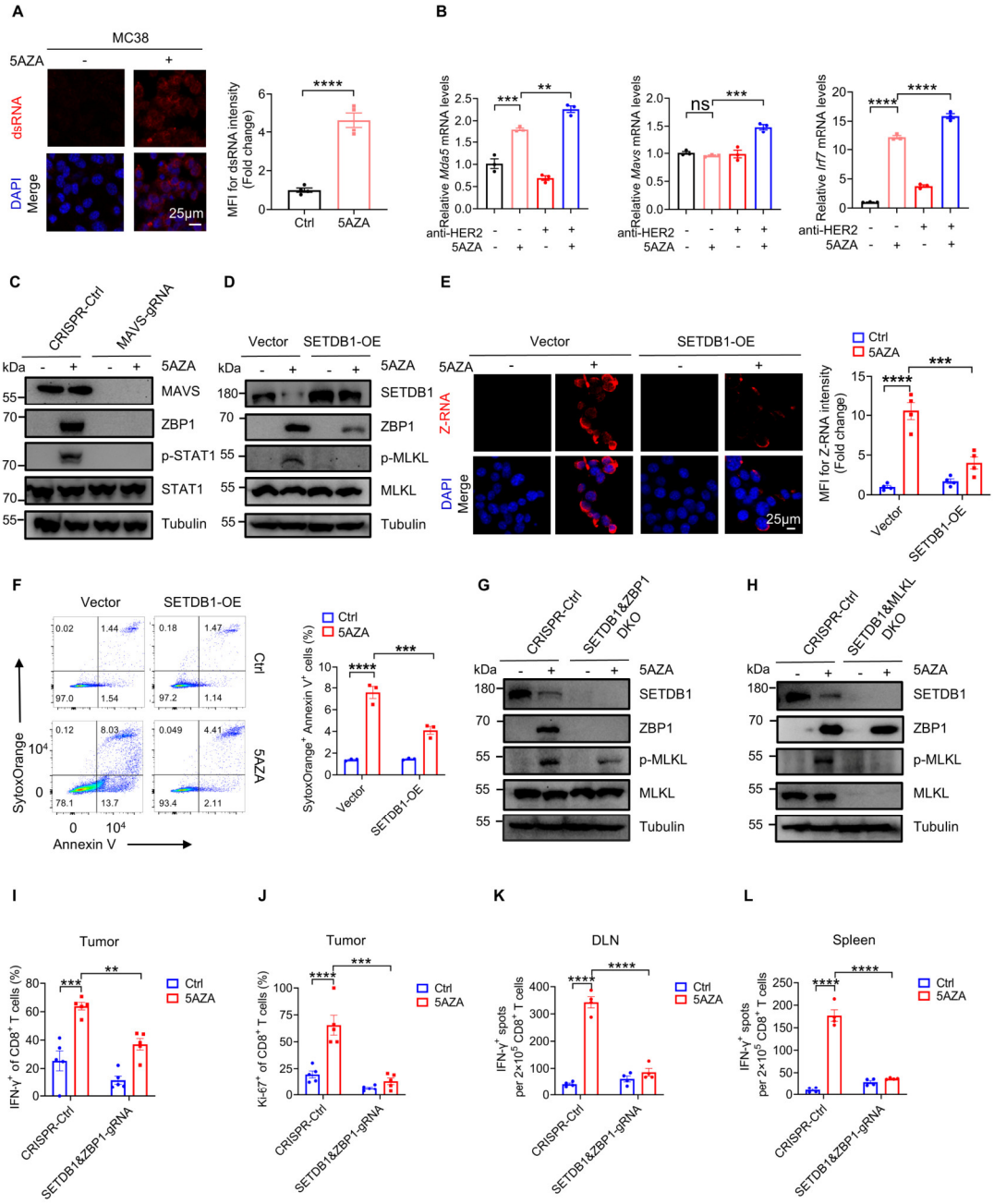

Figure S4. ZBP1 is necessary for SETDB1 inhibition-mediated efficacy after 5AZA treatment. Related to Figure 4. (A) IF staining of dsRNA in 5AZA-treated MC38 cells on day 5. Scale bar, 25μm. (B) Gene expression levels of *Mda5/Mavs/Irf7* pathway in TUBO cells after 5AZA monotherapy and combined treatment on day 5. (C) Western blotting of ZBP1 activation in MAVS-deficient MC38 cells under 5AZA treatment on day 5. (D) Western blotting of ZBP1-MLKL pathway in SETDB1-OE MC38 cells under 5AZA treatment on day 5. (E) IF staining of Z-RNA in SETDB1-OE MC38 cells under 5AZA treatment on day 5. Scale bar, 25μm. (F) Representative flow cytometric images and quantitative analysis of the percentage of SytoxOrange$^+$ Annexin V$^+$ cells in SETDB1-OE MC38 cells after 5AZA treatment on day 5. (G-H) Protein expression of ZBP1-MLKL pathway in SETDB1&ZBP1 and SETDB1&MLKL DKO

MC38 cells after 5AZA treatment on day 5. (I-J) Quantification of function and proliferation markers of $CD8^+$ T cells from CRISPR-Ctrl and SETDB1&ZBP1$^{-/-}$ MC38 tumors after 5AZA treatment on day 16 (n=5). (K-L) Function of tumor antigen–specific $CD8^+$ T cells from the DLN and spleen of CRISPR-Ctrl tumor–bearing mice compared to SETDB1&ZBP1$^{-/-}$ MC38 ones on day 16 (n=4). Data are represented as means ± SEM. ** $P < 0.01$, *** $P < 0.001$ and **** $P < 0.0001$ by Student's t test in (A) and one-way ANOVA in (B, E-F and I-L).

Supplementary Figure 5

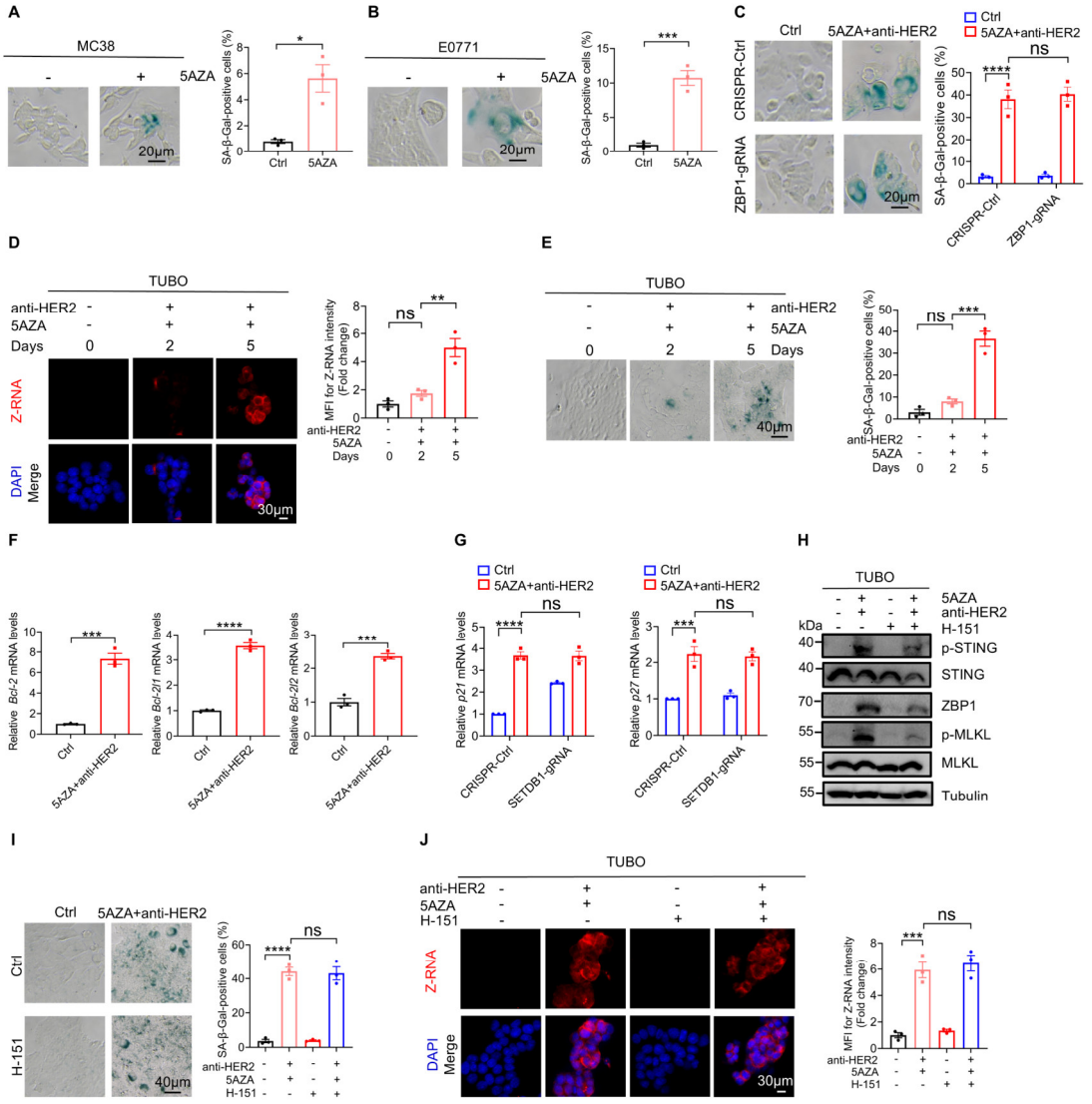

Figure S5. The combination of anti-HER2 mAb and 5AZA generated increased cellular senescence. Related to Figure 5. (A-B) SA-β-gal staining of MC38 and E0771 cells after 5AZA monotherapy on day 5. Scale bar, 20μm. (C) SA-β-gal staining in ZBP1-abrogating TUBO cells after combined treatments on day 5. Scale bar, 20μm. (D) Z-RNA formation in TUBO cells during time course of combined treatment. Scale bar, 30μm. (E) SA-β-gal staining in TUBO cells during time course of combined treatment. Scale bar, 40μm. (F) Gene expression levels of *Bcl-2* family in TUBO cells after combined treatment on day 5. (G) Expression levels of *p21* and *p27* in SETDB1-abrogating TUBO cells after combined treatments on day 5. (H) Expression levels of ZBP1-MLKL pathway in TUBO cells after combined treatment of 5AZA, anti-HER2 mAb and H-151 on day 5. (I) SA-β-gal staining in TUBO cells after combined treatment of 5AZA, anti-HER2 mAb and H-151 on day 5. Scale bar, 40μm. (J) IF staining of Z-RNA in TUBO cells after combined treatment of 5AZA, anti-HER2 mAb and H-151 on day 5. Scale bar, 30μm. Data are represented as means ± SEM. $^{*}P< 0.05$, $^{**}P < 0.01$, $^{***}P < 0.001$ and $^{****}P < 0.0001$ by Student's t test in (A-B and F) and one-way ANOVA in (C-E, G and I-J).

Supplementary Tables

Supplementary Table 1. Oligonucleotides used in this paper. Related to STAR Methods.

Gene names	Primers	Oligonucleotide (5'-3')
sgRNA oligos for gene deletion of tumor cell lines		
Murine *Zbp1* gRNA	Forward	AGTCCTTTACCGCCTGAAGA
	Reverse	TCTTCAGGCGGTAAAGGACT
Murine *Mlkl* gRNA	Forward	CGGAAACAATGCCAGCGTCT
	Reverse	AGACGCTGGCATTGTTTCCG
Murine *Setdb1*	Forward	CACCGAGGACTAAGACATGGCACAA
gRNA	Reverse	AAACTTGTGCCATGTCTTAGTCCTC
Murine *Mavs* gRNA	Forward	CACCGTTGGTGTCTCTCGTAAGCCA
	Reverse	AAACTGGCTTACGAGAGACACCAAC
qPCR Primers		
Murine *p21*	Forward	CAGACCAGCCTGACAGAT
	Reverse	TGACCCACAGCAGAAGAG
Murine *p27*	Forward	GGACCAAATGCCTGACTC
	Reverse	GGGAACCGTCTGAAACAT
Murine *Bcl-2*	Forward	GTCGCTACCGTCGTGACTTC
	Reverse	CAGACATGCACCTACCCAGC
Murine *Bcl-2-2l1*	Forward	GACAAGGAGATGCAGGTATTGG
	Reverse	TCCCGTAGAGATCCACAAAAGT
Murine *Bcl-2-2l2*	Forward	GCGGAGTTCACAGCTCTATAC
	Reverse	AAAAGGCCCCTACAGTTACCA
Murine *Mda5*	Forward	TCACTGATCTGCCCTCTCCT
	Reverse	CCTTCTCGAAGCAAGTGTCC
Murine *Mavs*	Forward	CTGCCTCACAGCTAGTGACC
	Reverse	CCGGCGCTGGAGATTATTG
Murine *Irf7*	Forward	CACCACACTACACCATCTACCTG
	Reverse	AGAGACTGTTGGTGCTAGACAAG
Murine *Gapdh*	Forward	CTCCACTCACGGCAAATTCAAC
	Reverse	GTAGACTCCACGACATACTCAGC